NASA CR-54339

HIGH TEMPERATURE MEASURING DEVICE

by

E. H. Carnevale, L. C. Lynnworth and G. S. Larson

prepared for

NATIONAL AERONAUTICS AND SPACE ADMINISTRATION

CONTRACT NAS 3-5201

PARAMETRICS, INC.

NOTICE

This report was prepared as an account of Government sponsored work. Neither the United States, nor the National Aeronautics and Space Administration (NASA), nor any person acting on behalf of NASA:

A.) Makes any warranty or representation, expressed or implied, with respect to the accuracy, completeness, or usefulness of the information contained in this report, or that the use of any information, apparatus, method, or process disclosed in this report may not infringe privately owned rights; or

B.) Assumes any liabilities with respect to the use of, or for damages resulting from the use of any information, apparatus, method or process disclosed in this report.

As used above, "person acting on behalf of NASA" includes any employee or contractor of NASA, or employee of such contractor, to the extent that such employee or contractor of NASA, or employee of such contractor prepares, disseminates, or provides access to, any information pursuant to his employment or contract with NASA, or his employment with such contractor.

Requests for copies of this report should be referred to

National Aeronautics and Space Administration
Office of Scientific and Technical Information
Attention: AFSS-A
Washington, D. C. 20546

NASA CR-54339

FINAL REPORT

HIGH TEMPERATURE MEASURING DEVICE

by

E. H. Carnevale, L. C. Lynnworth and G. S. Larson

prepared for

NATIONAL AERONAUTICS AND SPACE ADMINISTRATION

February 1, 1965

CONTRACT NAS 3-5201

Technical Management
NASA Lewis Research Center
Cleveland, Ohio
Advanced Development and Evaluation Division
Miles O. Dustin

Parametrics, Inc.
221 Crescent Street
Waltham, Massachusetts 02154

HIGH TEMPERATURE MEASURING DEVICE

by

E. H. Carnevale, L. C. Lynnworth and G. S. Larson

ABSTRACT

Investigations of an ultrasonic pulse technique for measuring the average gas temperature in a nuclear rocket engine are presented. This includes a study of sound propagation in high temperature gases, particularly hydrogen, and the effects of the nuclear rocket engine environment on the ultrasonic sensors. A working model, designed and constructed to illustrate the concepts and operation of a pulsed ultrasonic thermometer, is also described.

TABLE OF CONTENTS

TABLE OF CONTENTS (cont'd)

I. SUMMARY

24568

The object of this work is to investigate an ultrasonic pulse technique for measuring exhaust gas temperature in a nuclear rocket engine. Sound propagation studies include a theoretical analysis of the dependence of sound velocity on temperature, pressure, frequency, internal states, flow, boundary layers, and contaminants. Sound propagation studies also review the principle of ultrasonic temperature measurement, in terms of equipment functions.

A major portion of the work concerns environmental studies. Here, sound propagation was evaluated while simulating various parameters of the nuclear rocket engine environment. The effects of high neutron and gamma radiation on piezoelectric transducers were measured in the MIT nuclear reactor. During a 15 hour test, the flux levels were: thermal neutron flux, $\sim 2 \times 10^{13}$ n/cm^2-sec; flux of 1 Mev or greater energy neutrons, $\sim 2 \times 10^{12}$ n/cm^2-sec; gammas, 0.7 Mev average, 1.5×10^8 R/hr $\approx 10^{14}$ Mev/cm^2-sec. The geometrical and mechanical problems of conveying ultrasound to and propagating diametrically across a 1 to 2 ft gas path are considered. The gas, hydrogen, has a temperature up to 5000°R, and a pressure up to 600 psia. To determine the effects of vibration on the signal to noise ratio, an ultrasonic receiver and test unit were subjected to audio frequency accelerations ranging up to $\pm$ 10g. From these various environmental studies, it is concluded that temperature measurement by the ultrasonic pulse technique appears applicable to the nuclear rocket engine exhaust gas.

To demonstrate the ultrasonic system characteristics, a working model was constructed. The working model consists of a pulser, transducers, probes and receiving circuitry with meter readout to indicate gas temperature. It is estimated that an ultrasonic thermometer can measure exhaust gas temperature to within 2%.

II. INTRODUCTION

A. Background

Practical operation of a nuclear rocket engine requires measurement and control of core temperature. One approach to this problem is to measure the average temperature of the working gas after it has been heated by passage through the core, as indicated schematically in figure 1.

Measurement of high temperature gases have not kept pace with recent advances in high temperature technology. Although many theoretically feasible techniques of measuring high temperature gases have been suggested by a number of investigators, most of these need to be perfected and demonstrated before they can be accepted as reliable and be used on a routine basis. Furthermore, a technique applicable for one system may not be applicable for a different system. Thus, the specific requirements of a given system must first be considered before applying one or more of the many temperature measuring techniques that have been proposed.

Some of the difficulties associated with gas temperature measurement above 2500°R are summarized briefly by Sutton[1]. Sutton, in the one paragraph he devotes to gas thermometry, indicates that several optical measurements have been made. These optical measurements, however, do not appear feasible in the nuclear environment of concern here.

B. Ultrasonic Approach to Thermometry

An ultrasonic method is described in IIIB which has been used previously to determine the temperature of gases and plasma jets. Several studies carried out by the authors[2-5] have demonstrated the feasibility and the practicality of the method for temperature determinations in rarefied gases, hot gases, and in dc and ac plasma jets for temperatures up to 20,000°R.

C. Purpose of Investigation

The purpose of the present investigation was to determine whether the ultrasonic pulse method appears feasible in measuring gas temperatures in a nuclear rocket engine.

D. Scope of Work

Ultrasonic measurements were conducted during the simulation of nuclear rocket engine environmental parameters such as nuclear radiation, geometrical restrictions, high temperature, and vibration. Based on these experiments, a working model was constructed. This model demonstrates the feasibility and operation of an ultrasonic system which is applicable to nuclear rocket engine exhaust gas thermometry.

Complementing the experimental program, sound propagation in hydrogen was analyzed in order to predict, as far as possible, the effects of temperature, pressure, frequency, internal states, flow, boundary layers and contaminants on sound velocity.

The following sections and appendices discuss in some detail the sound propagation studies, environmental studies, and the working model.

The significance of the first year's work is that the ultrasonic pulse technique appears feasible for measuring exhaust gas temperature of a nuclear rocket engine.

III. SOUND PROPAGATION STUDIES

A. Theory of Ultrasonic Thermometry

Although the use of sound velocity in temperature determinations had been suggested nearly a century ago[6], relatively few measurements have been obtained with this method. Early work on this method was carried out by C. G. Suits[7] at General Electric in determining arc temperatures. In recent times it has successfully been applied to the measurements of gas temperature in an internal combustion engine[8], various gases[5], and high intensity dc and ac arc plasma jets[2-4].

In an ideal gas the dependence of the velocity of sound on temperature is given by $v^2 = \gamma RT/M$, where v is the sound velocity, γ is the ratio of specific heats, C_p/C_v, R is the gas constant, T is the temperature, and M is the average molecular weight. A measurement of sound velocity will lead to a determination of the temperature if the composition of the gas is known. This information is available for many gases (air[9], argon[10], hydrogen[11], etc.) at high temperatures so that one can calculate the sound velocity as a function of temperature.

In a real gas one must also take into account the frequency dependence of the sound velocity which arises from the finite relaxation times required for the adjustment of the internal degrees of freedom of the gas during an adiabatic acoustic compression. This phenomenon has been considered by several investigators[2, 12]. Velocity dispersion in hydrogen is discussed in appendix A1.

At present, in the absence of realistic estimates of the contribution of dissociation-recombination and vibration relaxation, the sound velocity in hydrogen has been plotted as a function of temperature and pressure with only rotational relaxation contributing fully to the specific heat (figure 2).

It should be noted that an absolute calibration of the high temperature, high pressure hydrogen system will ultimately be required since the contributions due to all of the internal states is unknown to the accuracy required.

The effect on velocity of boundary layers and the expected contaminants can be shown to be negligibly small (appendix A3, 4).

Nozzle geometry directs exhaust gas flow components across the measurement location, figure 1, such that the sound pulse propagates partly with and partly against flow components normal to the axis. Even at high gas velocities, however, this can lead to sound velocity errors no larger than 1%. When a correction is applied, based on the approximate velocity distribution, the error due to flow should be $< 0.1\%$ (appendix A2).

B. Principle of Measurement

The ultrasonic pulse system proposed for temperature measurements and monitoring in a nuclear rocket engine is shown in the simplified block diagram, figure 3. The object of this system is to provide an output signal proportional to the sonic transit time in the gas, which, in turn, is a function of the gas temperature.

The timing unit provides a trigger simultaneously to the pulse generator and the time integrator. The high voltage pulse (from the pulse generator) is converted to an ultrasonic pulse by the piezoelectric transducer. The sound is transmitted through the sonic probe, across the gas path, through the receiving sonic probe and then to the receiving transducer which converts the sound back into an electrical signal. The signal after amplification is fed to a trigger circuit which produces an output pulse when the received signal reaches a predetermined level. This pulse stops the integration process. In this way an output voltage is developed which is a function of the time between the transmitted and received signal. This time is the sum of the electrical time delays, the sonic transit time through the sonic probes, and the sonic transit time through the gas. Since the electrical time delay is constant and the sonic transit time through the sonic probe can be held constant (or measured), the output voltage is a function of the sonic transit time through the gas and thus a function of the temperature and can be properly calibrated. The voltage, in turn, can be used in a number of ways, e. g. , to record gas temperatures or to act as an error signal in a control system.

The sonic probes, which may require some cooling, should not be significantly affected by the high temperature, high pressure and high radiation during the total operation time. The acoustic properties of a transducer material such as quartz would not be altered more than $\sim 5\%$ under the assumed high radiation[13]. Other piezoelectric materials, particularly the more active lead-zirconate-titanate ceramics (Clevite's PZT-5) are also satisfactory for at least 1/10 of the assumed neutron

and gamma fluxes, based on tests in the MIT reactor, described below.

A further important consideration is the response time associated with an ultrasonic pulse method. One of the chief advantages of this method is the fact that equilibrium need not be established between the measuring instrument and the high temperature gas since the gas itself is used as the indicator. The sound velocity in hydrogen at room temperature is about 10^5 cm/sec and it increases with an increase in temperature. Hence, the sonic transit time through the hydrogen gas is extremely short, less than 0.5 milliseconds at room temperature, and less than 0.2 milliseconds at 5000°R for a 2 ft path length. Therefore, the response time can be < 1 msec, well within the required half second.

In the present application, another advantage of the ultrasonic method is that it provides a measurement of an <u>average</u> gas temperature between the probes.

IV. ENVIRONMENTAL STUDIES

This section and the related appendices describe the effects on sound propagation due to nuclear radiation, geometrical and mechanical restrictions, high temperature and pressure, and vibration. It will be shown that, based on our tests in simulated environments, and other available information, the nuclear rocket engine environment does not seriously degrade the ultrasonic thermometry system. The important conclusion, then, is that despite the severe environment listed below, ultrasonic thermometry appears feasible for exhaust gas temperature determination.

Let us assume the following conditions about a nuclear rocket engine:

1. The working gas is hydrogen.
2. The gas temperature can be as high as $5000^{\circ}R$.
3. The gas pressures can be as high as 40 atm.
4. Gas velocity up to 800 ft/sec.
5. "High" neutron and gamma flux present: 5×10^{13} n/cm^2 -sec and 10^{15} Mev/cm^2 -sec.
6. Noise level - 175 db.
7. Nozzle dia $\approx$2 ft at measurement location.
8. Wall temperature $\approx 2000^{\circ}R$.

These conditions have been grouped into four general environmental categories, as reported below. The problem is to measure continually and reliably the average gas temperature with a response time (response of the output signal to a temperature variation) of less than 0.5 sec.

A. Nuclear Radiation Effects on Piezoelectric Transducers

The object of this study was to determine which piezoelectric materials could operate in the proposed sensor, under intense and prolonged nuclear radiation. Candidate piezoelectric transducers were first compared on the basis of Curie point, transmitting activity, receiving sensitivity, availability, and the difficulty of handling after

prolonged irradiation. Based on these criteria, and preliminary radiation test results in the MIT nuclear reactor, it was decided to conduct a prolonged (15 hr) radiation test on PZT-5.

An ultrasonic unit was designed to fit into the most intense radiation facility in the MIT reactor. In this facility, the thermal neutron flux was 2×10^{12} n/cm^2 - sec (in 15 hr, 10^{18} nvt), the flux of 1 Mev or greater neutrons was 2×10^{12} n/cm^2 - sec (10^{17} nvt), and the gamma dose rate was 10^{14} Mev/cm^2 -sec. No significant transducer degradation occurred during the 15 hr test. Furthermore, twelve days after irradiation, a second test showed that the PZT crystal retained essentially all of its piezoelectric character. Details of the radiation tests are given in appendix B1.

Based on our PZT-5 radiation experiments in the MIT reactor, and the quartz crystal work of Truell et al[13] in the Brookhaven reactor a few years ago, it appears that both these piezoelectric transducer materials can operate in the radiation environment of a nuclear rocket engine.

It may be noted that, if necessary, the piezoelectric transducers may be withdrawn to a region of lower nuclear radiation, provided waveguides are used to convey the pulses to and from the measurement location. Appendix B2, part c, contains a waveguide analysis.

B. Geometrical and Mechanical Restrictions

The nozzle construction and dimensions, and the mechanical sealing requirements, impose limitations on the size, shape and mounting details of the ultrasonic probes. Ideally, the thermometry sensor would disturb neither the gas nor the nozzle. As a practical matter, however, it may be necessary for the probe elements to protrude slightly into the gas stream.

To facilitate mounting of the probe to typical tubular nozzles, the probe shape will initially be a vane or fin type. Thin lenticular vanes, approximately 1/10 in. wide x 1 in. long, will be brazed or welded to or between adjacent tubes. Vanes may protrude slightly into the gas stream, depending on boundary layer and heat transfer considerations.

It appears that W, W-Rh, Mo, stainless steel, Inconel, or

Inconel-X, are most attractive as probe elements. Aluminum probes were used in the initial tests of the working model. The ultrasonic waveguide or waveguides, if required, would probably be made of aluminum rod, strip or tubing.

In the working model, PZT-5 transducers are used. Refraction effects using both longitudinal and transverse modes have been evaluated.

Details of the probe and transducer designs, including a waveguide analysis and beam pattern study, are given in appendix B2.

It is concluded that there is at least one way of mounting the probes to overcome geometrical and mechanical restrictions imposed by the nozzle.

C. Temperature, Pressure

In this section, ultrasonic measurements at high temperature and pressure are described.

To test the validity of the equation giving the sound velocity in an ideal gas, $v = \sqrt{\gamma RT/M}$, velocity and temperature were simultaneously measured. The measurements spanned the range from room temperature to about 2300°R, near atmospheric pressure. To extend the temperature and pressure range to 5000°R and several hundred psi, a graphite oven can be used (figure 5).

Velocity and temperature measurements were conducted in a Hevi-Duty resistance wire furnace (figure 4). The test gases, contaminant free argon, nitrogen and helium, were heated to ~2300°R in a 36 mm dia Vycor tube. Ultrasonic pulses were transmitted through the gas by cylindrical probes. The probes were uncooled at the point of measurement, to avoid temperature gradients. Probe material has been steel at the lower temperatures, and fused silica up to the higher temperatures.

Sound velocity and thermocouple measurements were made simultaneously, and the results verified the equation, $v = \sqrt{\gamma RT/M}$. Furthermore, these tests permitted preliminary evaluation of probes, seals, fittings and mounts at elevated temperature, and also showed that under these rather ideal conditions, ultrasonic thermometry may be expected to yield temperature accurate to better than 1%.

D. Vibration, Noise

Adequate information on gas borne and rocket borne noise at megacycle frequencies is not available. This conclusion was reached after reviewing several recent papers on rocket and jet noise, and contacting individuals most likely to have the required information. For example, K. Eldred[17] reviewed his Huntsville measurements on rocket noise for Saturn type rockets. He feels that wall vibrations at megacycle frequencies will be negligibly small. Eldred points out that most rocket noise measurements have been conducted in air, on the ground, at zero rocket velocity, in the presence of deflectors, at frequencies below 20 kc.

In other recent work, Tedrick[18] notes that the apparent noise sources are mostly distributed along the supersonic portion of the jet. The higher frequency sources, he continues, are apparently near the mouth of the rocket engine, while the lower frequencies are generated farther downstream[19,20]. Now in the present study, the acoustic noise of importance is that between the reactor and the nozzle throat. It would appear that most of the noise could not get back to the region of temperature measurement.

However, it is important to note that there have been no measurements in this region. For example, a recent acoustical study of K1W1 B used measurements no closer than 100 ft from the reactor. These tests were conducted under hot flow conditions, to determine directivity and total radiated acoustic power. Measurements covered the band between 20 cps to 10 kc, with little information available at 25 kc. It would appear extremely difficult to extrapolate from presently available data to predict the sound field near the temperature sensors. In approaching this region, Manhart[21] points out that phase relationships get rather complicated, and so an empirical solution would be required.

One therefore draws the following conclusions:

1) There is no applicable data;

2) There is very little data from which one can extrapolate to the present problem;

3) In applications where ultrasonic vibrations become important, it will be necessary to measure their spectral distribution well beyond the range of conventional sound level meters or accelerometers, in the presence of high temperatures and high flux levels, with adequate simulation of flight conditions.

Since it is probably impossible to simulate realistic vibration and noise conditions in any ground test, it was decided, for simplicity, to simulate in part the effects of audio frequency rocket borne noise on the ultrasonic transducer with a routine vibration test.

A 2.5 mc ultrasonic unit, essentially the same as that used in the radiation tests, was constructed. The unit was tested at 500 cps to $\pm$ 7g, and at 2000 cps to $\pm$ 10g, at Associated Testing Labs of Burlington, Mass. Vane probes were also used in these tests, together with 2.5 in. dia PZT-5 crystals resonant between 300 kc and 3 mc.

Prior to these tests, it has been predicted that by combining mechanical and electrical filtering most of such audio frequency noise would be eliminated. The tests confirmed this prediction. Noise was readily filtered to below 1 mv. Details on the vibration test, and acoustical and electrical filtering, are given in appendix B3. In these tests, the 1 mv noise level was 66 db below the 70 v signal (S/N = 2000). In a nuclear rocket engine, the S/N ratio is expected to exceed 10, which means the signal would be 20 db above the noise (see also appendix C).

V. WORKING MODEL

The principle of temperature measurement using pulsed ultrasound is discussed above. To demonstrate the operation of a pulsed ultrasonic thermometer, a working model has been constructed. This model was designed to work in air, over paths up to about 1 ft (figure 6), for demonstration and test purposes.

The transmitter is driven by a pulsed oscillator between about 500 kc and 3 mc. Pulse length is about 25μs, and pulse amplitude about 200 volts rms, from an output impedance of 93 Ω. The crystals are PZT-5, either 2.5" diameter, or several rectangular slabs, each about 0.1 in. x 1 in. in area. Crystal thickness is $\lambda/2$ (i.e., at 500 kc, about 0.165 in.).

The receiving circuits include a tuned amplifier, filter and integrator. The output meter deflects proportional to transit time.

A variety of probes may be used with this working model, including vane types, of aluminum or stainless steel.

Details of working model system characteristics, preliminary calibration, estimation of signal to noise ratio and accuracy, are given in appendix C.

APPENDIX A

Sound Propagation Studies

1. Theoretical Sound Velocity in Hydrogen

In an ideal gas, the dependance of the velocity of sound on temperature is given by

$$v^2 = \gamma RT/M ,$$

where v is the sound velocity, γ is the ratio of specific heats C_p/C_v, R is the gas constant per mole, T is the absolute temperature, and M is the average molecular weight. A measurement of the sound velocity will lead to a determination of the temperature if the composition of the plasma or gas is known. In a real gas, one must take into account the frequency dependance of the sound velocity, which arises from the finite relaxation times required for the adjustment of the internal degrees of freedom of the gas during an adiabatic acoustic compression; thus, equilibrium between the various degrees of freedom is not established at the higher frequencies and a dispersion of velocities results. This dispersion is due to a time dependance of the specific heat at constant volume. This phenomenon has been considered by several investigators[2, 12]. In general, if a particular process occurs with the relaxation time τ_r, it will produce a velocity dispersion for sound waves in the neighborhood of the relaxation frequency:

$$\nu_r = 1/(2\pi\tau_r) .$$

For sound frequencies which are far from any of the relaxation frequencies, the sound velocity will be given by the usual formulas for a nonrelaxing gas, except that those processes which are too slow to follow the sound wave are neglected in calculating the gas properties.

In the case of hydrogen over the temperature and pressure range of interest in this study it is necessary to consider the energy going into dissociation, vibration and rotation of the molecules.

The rotational relaxation frequency in hydrogen at room temperature and atmospheric pressure has been experimentally determined to be about 10 mc/sec[12]. This rotational relaxation frequency would shift by the ratio of p/η where p is the pressure and η is the viscosity[12]. At 2800°K and 600 psi the rotational relaxation frequency would be ~100 mc/sec.

In the case of dissociation the relaxation frequency is roughly estimated to be $\lesssim$0.5 mc/sec at high temperature and high pressure with a contribution to the specific heat of about 0.2R. At 1 mc/sec only part of this specific heat would contribute to the sound velocity.

The vibration relaxation frequency at high temperature and high pressure has been very roughly estimated to be of the order of 1 mc/sec, with a contribution to the specific heat of about 0.7R.

Of the above internal energy states considered, only rotation definitely contributes to the specific heat under all conditions of temperature and pressure.

At present, in the absence of realistic estimates of the contribution due to dissociation and vibration the sound velocity in hydrogen has been plotted as a function of temperature and pressure with only rotational relaxation contributing fully to the specific heat (figure 2).

It should be noted that an absolute calibration of the high temperature, high pressure hydrogen system will ultimately be required since the contributions due to all of the internal states are unknown to the accuracy required. This calibration can be accomplished in a high temperature, high pressure oven, figure 5, similar to that described by Pears et al[22].

2. Effect of Gas Flow Components Parallel and Anti-parallel to Sound Pulse Velocity Vector.

The nozzle's converging section deflects some of the initially axial flow. As a result, near the transmitter, there is a component of gas flow parallel to the sound beam, increasing the measured average sound velocity. Near the receiver, there is a component of gas flow opposite the sound beam, decreasing the measured average sound velocity below the value that would be obtained under no flow conditions. It is shown below, subject to several simplifying assumptions, that even

if such flow effects are not compensated for, the indicated temperature may be less than the true average temperature only by about 1% or less. If the gas flow velocity distribution is known, then the errors due to flow can be reduced to $< 0.1\%$.

In figure 1, let us first assume that the acoustic path across the diameter is twice the throat diameter D. Second, let us assume that the converging walls are inclined such that the gas flow components parallel and antiparallel are about 1/10 of the undisturbed sound velocity c. Third, let us assume that these flow components exist only between the conical, converging section and an imaginary circular cylinder tangent to and coaxial with the throat. That is, the flow affects the sound velocity over a path length D/2 near the transmitter, and D/2 near the receiver.

The sonic transit time over the path D/2 between wall and imaginary cylinder, near the transmitter, is

$$t_T = \frac{D/2}{c + 0.1c}$$

Near the receiver, over the path D/2, the transit time is

$$t_R = \frac{D/2}{c - 0.1c}$$

Across the imaginary cylinder, the transit time is

$$t_c = \frac{D}{c}$$

The total transit time is

$$t = t_T + t_c + t_R$$

$$= \frac{D}{2.2c} + \frac{D}{c} + \frac{D}{1.8c}$$

$$= \frac{D}{c} \quad (2.01)$$

The indicated average velocity is

$$c_I = \frac{2D}{t} = \frac{c}{1.005} \simeq c\ (1 - .005)$$

For this case, then, the indicated sound velocity is 1/2% too low, corresponding to the indicated temperature being 1% too low.

A more realistic model of the gas flow would show that the indicated temperature is less than the average temperature by only a fraction of 1%. Again, the error can be reduced to < 0.1% by compensating for the flow distribution.

3. Boundary Layer Calculation

The following calculation considers only that boundary layer due to the protrusion of cooled probes into a hot gas stream. The transit time error due to cool boundary layers may be estimated as follows. According to Schlichting[23], if a cool probe projects into a high temperature stream, a cooled boundary layer is produced, having a thickness δ given by the approximation

$$\delta = \sqrt{L\eta / \rho u}$$

where L = distance from leading edge,

η = viscosity in undisturbed flow,

ρ = density in undisturbed flow,

and u = flow velocity.

For the conditions of interest to this contract, a one inch probe will produce a boundary layer δ of about 10^{-3} cm. As a result the ultrasonic pulse will be "smeared" by about 0.02μsec in a total transit time of about 150μsec. This time uncertainty is negligibly small. For smaller diameter probes, the "smearing" is even less, since δ is proportional to the square root of L.

Besides the probes, the cooled nozzle wall produces a boundary layer too. If the flow is laminar, this boundary layer would be negligibly thin. If the boundary layer is turbulent, its thickness is diffi-

cult to estimate. If it becomes necessary to avoid the effects of a turbulent boundary layer, various approaches may be taken, for example, using protruding probes of a suitable contour.

4. Effect of Contaminants

In an earlier study[5] of the effect of contaminants on the sound velocity in a plasma jet, it was determined that gaseous contaminants produce a percentage change in velocity equal to approximately the contaminant percentage by weight.

Particulate contaminants would have negligible effect on velocity. They would act primarily as scattering centers, their relatively high acoustic impedance preventing any measurable signal from being propagated through them.

In summary, if the contaminant level were of the order of 0.1% or less, then velocity would be in error by a corresponding 0.1% or less.

APPENDIX B

Environmental Studies

1. Nuclear Radiation Effects on Piezoelectric Transducers

a. Preliminary tests in the MIT nuclear reactor

At MIT's request, samples of cable, piezoelectric crystals and glycerol were irradiated for intervals up to 2 hours, to determine activation levels and to determine the behavior of isolated parts of the anticipated ultrasonic experiment.

With respect to safety and handling requirements, these tests indicated that quartz and PZT-5 crystals are preferable piezoelectric elements, that glycerol is a suitable couplant, and that Aljak is a reasonable cable, for radiation exposures up to one day. These preliminary tests, then, provided the information necessary for a prolonged test. Again, the objective of prolonged monitoring of PZT-5 (one of Clevite's lead-zirconate-titanates) in a high neutron and gamma flux field was to determine this material's suitability for

use in an ultrasonic temperature sensor in a nuclear environment.

b. Design of Ultrasonic Experiment Suitable for Prolonged Testing in Most Intense Flux in MIT's Reactor.

The most intense neutron and gamma fluxes in the MIT reactor have been measured in Position 13[24]. In this position, the neutron flux of energy > 1 Mev is 1.73×10^{12} n/cm^2-sec. The neutron flux between 0.01 and 1 Mev is 1.68×10^{13} n/cm^2-sec. Their sum, 1.85×10^{13} n/cm^2-sec, represents the total neutron flux of energy > 0.01 Mev. The gamma dosage is 1.5×10^{8} R/hr or 10^{14} Mev/cm^2-sec (0.7 Mev average).

An ultrasonic experiment designed to test a cable, connector, crystal, couplant and buffer rod for 15 to 24 hours in Position 13 is shown in figure 7. The aluminum jacketed cable can be heliarc welded, or bonded with epoxy (such as Ciba's Araldite 502 + hardener 951) to the aluminum cavity. Before screwing the assembly together, the threads are coated with stopcock grease, to seal the assembly against the heavy water in which it will be immersed in Position 13. Figure 7 shows that the ultrasonic unit is the same size as the aluminum can normally used in MIT's reactor studies. Hence, the unit can fit next to a fuel element in Position 13. To avoid possible overheating, the ultrasonic unit was immersed in heavy water throughout the test.

c. Block Diagram

A block diagram of the irradiation experiment is given in figure 8. Note that the full oscillator voltage, about 600 volts peak to peak, was applied to the cable and crystal, in order to test for voltage breakdown.

Between the crystal and the receiver, the transmit pulse and the echo were both attenuated by 40 db during the 15 hour run. This avoided overloading the oscilloscope's amplifier, and anticipated a possibly large reduction in echo amplitude during the course of the test.

Specimen temperature was measured in two ways. First, a chromel-alumel thermocouple was peened into the tip of the cap, and its output was read periodically (figure 9, top) and recorded continually.

Second, the pulse transit time in the aluminum threaded rod was measured periodically. This transit time would have increased if the temperature rose significantly.

About 15 minutes after the ultrasonic unit was inserted in Position 13, a second Aljak cable was lowered alongside. This second coaxial cable was left open circuited as a control measure, so that in case no signals were obtained from the ultrasonic unit, one could determine whether the failure was due to the cable, or factors other than the cable.

d. Test Results (Figure 9)

Temperature. Temperature quickly rose from room temperature to 560 $\pm$ 5°R, but remained at this value until reactor cooling fans were slowed down as part of another MIT experiment (0800 hrs). It had previously been estimated that the temperature would not rise above 600°R, which is about 70°R below the softening point of the polyethylene used in the experiment. Monitoring the temperature, therefore, was mainly a precautionary measure. Results showed that the temperature predictions were quite reasonable.

Cable Resistance. The dc input resistances (between grounded shield and center conductor) of the test cable and the control cable were measured periodically, and found to be > 1 Meg Ω throughout the test. These Aljak cables, flexible and relatively uncontaminated with elements potentially transmutable into long half life isotopes, were selected because of their compatibility with Position 13 and handling requirements. Other cables would be used in an actual nuclear rocket installation.

Echo Amplitude. The echo amplitude is mainly a function of the activity and sensitivity of the PZT-5 crystal, and the coupling efficiency of the glycerol film between crystal and threaded rod.

When the ultrasonic unit was lowered into the thimble, the echo immediately fell ~6 db, then grew, and then fell again to -7 db, all within the first hour. During the next 14 hours, the echo was essentially constant, falling to -10db by the end of the test; i. e., a change of 3 db in 14 hours. These variations are believed due to the polyethylene backing member changing shape initially, leading to variations in the coupling pressure.

A subsequent test of the crystal twelve days after the 15 hour

irradiation period showed that the PZT-5 retained essentially all of its initial activity and sensitivity. This second test would seem to confirm that, in figure 9, the first hour fluctuations in echo amplitude were not due to the crystal, but rather to the polyethylene backing member.

In the working model, which is a through transmission measurement (not pulse echo, as in the MIT experiment), a backing member is not required.

e. Effect of 1 Mev Neutrons on Glycerol

A glycerol film is often used in conventional ultrasonic testing as a couplant between the transducer and a solid. Chemically, glycerol = $CH_2OHCHOHCH_2OH$, so that the breakdown into elements is as follows:

Element	Atoms/Molecule	Atomic No.	Atomic Weight	Approx. % by weight
C	3	6	12	40
H	8	1	1	10
O	3	8	16	50

The density of glycerol is ≈ 1 g/cc.

Under 1 Mev neutron irradiation, nitrogen may be produced by two processes:

$$C_6^{12}(n, e^-)N_7^{13}$$

and

$$O_8^{16}(n, e^+)N_7^{17}$$

The probability of change for each atom in time t by some process is

$$p = \sigma_T \phi t$$

where ϕ = 1 Mev neutron flux = 10^{13} n/cm^2-sec

$t = 10^{18}$ nvt/10^{13} n/cm^2-sec = 10^5 sec $\approx$28 hrs,

and σ_T = total cross section, barns

Element	σ_T	p (t = 28 hrs)
H	10×10^{-24} cm^2	10×10^{-6}
C	3×15^{-24} cm^2	3×10^{-6}
N	1.5×10^{-24} cm^2	1.5×10^{-6}
O	2×10^{-24} cm^2	2×10^{-6}

Conclusion:

Only 1 to 10 ppm of glycerol will transform or leave the molecule in 28 hours of bombardment with flux of 10^{13} n/cm^2-sec of 1 Mev neutrons.

f. Dose Rate to Flux Conversion for Gammas in Reactor

The energy transmitted through x(g/cm^2) of air for absorption coefficient a(cm^2/g) is

$$E = E_o e^{-ax}$$

where E_o(Mev/cm^2-g) is input flux and E(Mev/cm^2-g) is output.

$$\left| \frac{dE}{dx} \right| = E_o a e^{-ax} \approx E_o a$$

$\left|dE/dx\right|$ is energy absorbed per gram per sec, that is, the dose/sec.

Thus

$$\alpha E_o = D_s \text{ (Mev/sec-g)}$$

$$E_o = D_s/\alpha$$

Now, 1 Mev/g (10^{+7} x 5.24) = 1 R (Roentgen in air)

Thus

$$E_o = \frac{5.24 \times 10^7}{\alpha_{air}} D_s \text{ (R/sec)}$$

For air $\alpha = 0.03 \text{ cm}^2/\text{g}$. Thus

$$\text{(air) } E_o = \frac{5.24 \times 10^7}{3 \times 10^{-2}} D_s \text{ (R/sec)}$$

$$E_o \text{ (Mev/cm}^2\text{-sec)} = 1.75 \times 10^9 D_s \text{ (R/sec)}$$

For the position of interest in the MIT reactor, the dose rate is:

Position 13: $D_s = 1.5 \times 10^8$ R/hr = 4.17×10^4 R/sec.

Therefore

$$E_o \text{ (Position 13)} = 1.75 \times 10^9 (4.17 \times 10^4)$$

$$= 7.3 \times 10^{13} \text{ Mev/cm}^2\text{-sec.}$$

2. Geometrical and Mechanical Restrictions

a. Acoustic Short Circuit

A schematic diagram of a nuclear rocket engine is given by Sutton[25], and in further simplified manner, in figure 1. In some cases of interest, the thrust chamber may consist of brazed, liquid hydrogen cooled tubes. These tubes may be reinforced with one or two exterior bands or sheets, to withstand the chamber pressure. This construction and pressure requirement make it undesirable to pierce the thrust chamber to allow for sensor insertion. However, the continuity of the reinforcing band, and perhaps even the tubing, are such that acoustic signals may propagate around the nozzle, and interfere with reception of the acoustic signal transmitted diametrically across the gas.

To minimize the effect of the acoustic short circuit, it will be necessary in some cases to acoustically isolate the probes from the nozzle. Acoustic isolation may utilize an alternating series of acoustically dissimilar materials[8], and/or an acoustic delay between probe and nozzle, with minimal contact area between probe and nozzle[4]. These approaches require piercing at least part of the thrust chamber, i.e., the reinforcing panels.

b. Vane Probes

One method of acoustic isolation would use vane probes, as shown in the foreground of figure 6, and also schematically, in figure 1. The vanes may either contact the outer surface of the tubing, or protrude between cooling tubes into the exhaust gas. Propagation through brazed tubing has been demonstrated in a preliminary experiment (figure 10).

Referring to figure 1, if the vanes do not protrude, but radiate through the tubing, then the ultrasonic beam in hydrogen is required to refract about 45° from the normal. For the refracted ray in $5000^{\circ}R$ hydrogen to be refracted 45° from the normal, the incident velocity v_1, and angle θ_1, must satisfy Snell's law:

$$\frac{v_1}{\sin \theta_1} = \frac{v_{hydrogen}}{\sin 45^{\circ}} = \frac{0.4 \text{ cm}/\mu\text{sec}}{.707}$$

(1) Longitudinal Mode

Let us first consider materials whose longitudinal velocity $v_l < v_{hydrogen}$. Refer to figure 11. Solids of longitudinal velocity lower than hydrogen at 5000°R include materials such as graphite, Pb, $BaTiO_3$, plastics and elastomers. Flux levels rule out plastics and elastomers. $BaTiO_3$ suffers a phase transformation near 400°K, Pb has a low melting point and is highly attenuating to ultrasound, and graphite would be dubious because of strength and sealing problems.

Next, let us consider materials whose longitudinal velocity $v_l > v_{hydrogen}$. From Snell's law, we are limited to the range $1 < v_l/v_{hydrogen} < 1.414$, or $0.4 < v_l < 0.57$ cm/μsec. Again, from figure 11, available solids are few, but using room temperature velocities, there are three possibilities using refractory metals. Tantalum, for example, with $\theta_1 = 49°$, or colombium, with $\theta_1 = 40°$, or tungsten, with $\theta_1 = 34°$, appear reasonable. (In Mo [figure 11], $v_l > 0.57$ cm/μsec at room temperature).

We conclude that a vane probe is possible using probe materials in which the longitudinal velocity is up to 40% greater than the average sound velocity in the gas.

(2) Shear Mode

A refracted ray at 45° to the normal in hydrogen at 5000°R can also be achieved with a large number of flush mounted probe materials, provided one uses the shear mode, and the shear wave velocity in the probe is < 0.57, but $\neq 0.4$, cm/μsec. All refractory metals, plus many others, satisfy this criterion (figure 12). Stainless steel 347 or Inconel, with shear wave velocities of 0.3 cm/μsec, would be mounted so $\theta_1 = 32°$ (figure 13). These alloys are probably compatible with nozzle requirements.

Mode conversion from a shear wave in a solid to a longitudinal wave in a gas, although based on well-known acoustic principles, apparently has not been demonstrated previously. To demonstrate the concept, several experiments were conducted with angled probes in air. One of these experiments is illustrated in figure 14. Here the shear wave propagates in the aluminum probe at $v_T = 0.32$ cm/μs, and strikes the beveled face at $\theta_1 = 35°$. The emerging beam is longitudinal, and propagates in air at $v_L = 0.033$ cm/μs, about 1/10

of the incident velocity. Therefore, the beam is strongly refracted, θ_2 being about 1/10 of θ_1, or about 3°. In figure 14, the longitudinal wave is received by a 1 mc PZT-5 longitudinal mode crystal, after passing through the brazed stainless steel tube walls.

It is appreciated that if the sensor is to operate over the full temperature decade from 300 to 3000°K, then $v_{hydrogen}$ will vary by $\sqrt{10}$, i.e., from about 0.125 to 0.4 cm/μsec (figure 2). A single, fixed angle probe, then, would transmit pulses into the hydrogen at refracted angles that vary with temperature.

One approach to this problem is to use several probes, each designed for a narrow temperature range.

Another approach is to sacrifice the advantages of a non-protruding probe, and use protruding or recessed vanes. This solution avoids refraction by arranging the radiating faces parallel to the ultrasonic wavefronts, and requires longitudinal mode.

c. Acoustic Waveguides

(1) General

In the working model, the piezoelectric crystals are located as close as possible to the probe face. However, in some nuclear rocket engine applications, the radiation flux at the measurement location may degrade crystal performance. In such cases, it may be necessary to use an acoustic waveguide to convey the pulses to and from the measurement location. Waveguides permit one to withdraw the crystal to a region of reduced flux levels.

Waveguides increase the crystal-to-crystal transit time, and decrease the received signal amplitude. Noise level may increase slightly, but in vibration tests of an ultrasonic unit containing a waveguide several inches long, vibrated at $\pm$ 7g at 500 and 2000 cps, the signal to noise ratio was about 2000:1.

(2) Transit Time

The sound velocity in a waveguide depends on waveguide material, temperature distribution, radiation damage, and the ultrasonic mode being propagated. Longitudinal and shear wave velocities for a number of materials at room temperature are shown in figures 11

and 12. For example, the longitudinal mode transit time in Al, W, SiO_2 or steel waveguide, 10 ft long, is about 500 μs at room temperature. Sound velocity in solids is less sensitive to temperatures at low temperatures, and more sensitive at elevated temperatures approaching the melting point[29, 30].

When the temperature distribution and radiation effects on acoustic properties of the waveguide are known, the delay time in the waveguide can be calculated. In general, however, waveguide delay time would not be calculated, but would be measured ultrasonically during ground tests of a nuclear rocket engine.

Another approach is to monitor the waveguide delay time continually, while measuring the average gas temperature. This requires a pulse echo system for each waveguide, assuming unequal waveguides. Pulse echo transit time measurements do not have to be made at the same frequency as the gas measurement, and could easily be made at 10 mc, for example. Figure 3 indicates how an output is generated in the through transmission system. In the pulse echo systems the technique is essentially the same. Voltages are developed proportional to the transit time in each waveguide. These pulse echo "waveguide voltages" are subtracted from the total or through transmission "waveguide + gas voltage", the difference voltage being proportional to the transit time in the gas alone.

(3) Signal Amplitude

Waveguides reduce signal amplitude due to absorption, scattering and mode conversion. These factors, in turn, depend on waveguide material, temperature, radiation damage, ultrasonic frequency, surface finish, mode being propagated, and waveguide shape.

Experimentally, signal attenuation was measured at room temperature in solid aluminum rods (1 to 1.5 in. dia) and tubular conduit (3/4 in. dia EMT) at 500 kc. In the rod, the signal was reduced at the rate of 1 db/ft. In the tubing, the loss was 1/4 db/ft when empty, and also 1 db/ft, when filled with water (to simulate coolant). (The rod could be cooled in a coaxial system, or by winding a helix of cooled tubing around it, as is sometimes done with certain water cooled ultrasonic probes used in plasma studies[3, 4]).

In tubing experiments, it was found that sound travelled around 90° bends ($\approx$ 6 in. radius of curvature) without any additional loss.

Figure 19 shows the waveguides that were tested. The air path between waveguide and receiver represents a hydrogen path of several feet.

It is concluded that, if necessary, waveguides of cylindrical, tubular or strip configurations could be used in the nuclear rocket engine environment.

d. Beam Pattern

(1) Simple Sources

To minimize the disturbance of the nozzle when introducing sonic probes, it is desirable to make each probe element as small as possible. If a single probe element, small with respect to λ, radiates alone, then its beam diverges rapidly in the far field. However, several small probe elements can be arrayed to form a beam of controlled spread. The directivity functions for 2 and 3 simple or point sources, spaced up to 1λ apart, are plotted in Sonics[26]. For a simple dipole, the half-beam width is $\theta = \sin^{-1} (\lambda / 2d)$ where d is the spacing. For three simple sources, the half-beam width is $\theta = \sin^{-1} (\lambda / 3d)$.

(2) Piston Sources

Based on Huygen's principle, piston sources can be analyzed by integrating the differential contributions over the piston surface. For a square piston, the half-beam width is $\theta = \sin^{-1} (\lambda / d)$, where d is the edge of the square. For a circular piston, the half-angle of the main lobe is given by the Fraunhofer formula, $\theta = \sin^{-1} (1.22\lambda / d)$ where d is the piston diameter.

(3) Vane Probe - Strip Sources

Vane probes are shown in figure 6. Vane cross section dimensions are 0.1 in. x 1 in. Radiating into hydrogen at 5000°R, at 500 kc, each strip individually acts as a rectangular piston source of dimensions $\lambda / 3 \times 3\lambda$. To determine whether several vane elements could properly be treated as a piston source, the following experiment was conducted.

(4) Scaled Experiment in Air at 40 kc

In hydrogen at 5000°R and 500 kc, $\lambda \simeq 0.3$ in. In air at room

temperature, $\lambda \simeq 0.3$ in. at f ≃40 kc. To simulate the beam from 5 vanes radiating into hydrogen at 5000°R, a plate with 5 slits, 0.1 in. x 1 in. each, and 0.4 in. between slit edges, was illuminated at 40 kc with essentially plane waves. The slits then behave as 5 secondary sources whose beam pattern is readily measured. The experiment and observed main lobe beam pattern are shown in figure 15. Note that the observed zero very nearly coincides with the zeros at $\pm$ 11° predicted by the Fraunhofer diffraction formula. It is therefore concluded that the group of vanes act as one piston source. Furthermore, the far field beam spread of one or more vanes can be predicted with good approximation by the Fraunhofer formula, $\theta = \sin^{-1}(1.22\,\lambda/d)$, where now d is interpreted as the appropriate overall probe dimension. In the near zone, of length d^2/λ, beam spread is negligible. Finally, for a given d, the resultant amplitude is approximately proportional to the number of vane elements.

3. Vibration, Noise

a. Vibration Tests

To measure the noise generated in ultrasonic crystals and probes vibrated in the audio range, a vibration test was conducted at the New England Division, Associated Testing Laboratories, Inc., Burlington, Mass. on Nov. 4, 1964.

The vibration test system consisted of:

Vibration exciter, Calidyne, Model A-175;

Power amplifier and control console, Ling Electronics, Model CP-5/6;

Accelerometer, Endevco Corp., Model 2215-C.

A 2.5 mc ultrasonic unit, similar to that shown in figure 7, was vibrated at 500 and 2000 cps to $\pm$ 7g. Two mounting orientations were used, to achieve vibration components in direction parallel and perpendicular to the crystal axis.

The low frequency noise was proportional to the g level and vibration frequency. At $\pm$ 7g, before filtering, the 500 cps noise was 10 mv, and the 2000 cps noise, about 40 mv peak to peak. After simple constant - k filtering, the noise was reduced below 1 mv. During these tests, the 2.5 mc echo signal in the pulse echo probe was 70 volts peak

Figure 17 illustrates these types, and defines the symbols used in the following analysis.

(a) Shunt tuned filter

In figure 17a, if we assume the total series resistance of the circuit R is less than 1/10 of either reactance (i.e., $Q = \omega L/R > 10$) we may readily calculate the inductance L required for parallel resonance, as a function of crystal resonant frequency and area. At resonance,

$$\omega L = 1/\omega C$$

$$L = 1/\omega^2 C = 1/4\pi^2 f^2 C$$

Now $C = K\epsilon_o A/d$

At resonance $d = \lambda/2 = v/2f$

$$\therefore L = v/8\pi^2 K\epsilon_o A f^3$$

For PZT-5 we have $v \approx 0.15$ in./μsec

$K = 1500$

$\epsilon_o = 0.225 \times 10^{-12}$ fd/in.

$\therefore$ for PZT-5, $L = 6.35 \times 10^{12}/Af^3$

L is plotted as a function of f, with A as parameter, Figure 18. This plot indicates that the expected range of inductance values, ~0.1 to 100 μhy for f between ~1/2 mc to 2 mc is readily achieved in practice.

The width of the bandpass is

$$\Delta f = f/Q = fR/\omega L = R/2\pi L$$

and this can be controlled to some degree, in practice, by adjusting R_L. The response of a shunt tuned circuit is given by Terman's[27] universal resonance curve, for $Q = 10$, 25, and ∞.

to peak. That is, the signal to noise ratio was 70/0.04 or nearly 2000:1 at $\pm$ 7g.

Next, a 2.5 in. dia crystal receiver was vibrated as above (500 and 2000 cps to $\pm$ 7g) while receiving 300 kc pulses. These pulses were transmitted from a vane probe through an air path equivalent to several feet of hydrogen. The air borne 300 kc pulse signal was not degraded by the audio frequency vibration.

b. Filtering

(1) General

To reduce vibration effects, isolation and filtering techniques may be applied. In avoiding the acoustic short circuit (appendix B2) some of the noise will be prevented from reaching the transducer. In addition, the selectivity of mechanically and electrically resonant devices filters out the noise to a large degree. Figure 16 illustrates the range of passbands as a function of Q and frequency.

(2) Mechanical Filtering Techniques

The mechanical Q of PZT-5 is 75. This means that the transducer responds quite selectively to acoustic waves at its resonant frequency. For example, a transducer resonant of f_o = 500 kc has a bandwidth of $\Delta f \approx f_o / Q$ = 500 kc/75 $\approx$ 7 kc between half power points. That is to say, noise and vibration frequencies several kc away from f_o will be inefficient in exciting this crystal. Consequently, the influence of low frequency noise and vibration is small, due to the inherent mechanical selectivity of the crystal resonator.

(3) Electrical Filtering Techniques

To obtain a sufficiently high signal to noise ratio at the ultrasonic frequency of the sensor, it may be necessary to employ electrical filtering techniques. There are many types of electrical filters available. The choice principally depends on reliability of operation in the nuclear rocket environment, transmission characteristics and impedance considerations. We consider here only three types of passive electrical filters. These are;

1. Shunt tuned filter
2. Constant -k filter
3. Crystal filter

(b) Constant -k filter[28]

Figure 17b illustrates a bandpass constant -k ladder filter. The series resonant branches pass the ultrasonic frequency, but block other frequencies. The parallel resonant branch presents a high impedance to the ultrasonic frequency, but tends to short circuit other frequencies directly to ground. Typical element values have been calculated as a function of center frequency, bandwidth = 100 kc and nominal impedance R = 93 Ω. Results are tabulated in Table 1.

Table 1.

Inductor and Capacitor Values for Constant -k Filter.

Design Equations:

$$L_1 = R/\pi (f_2 - f_1) = R/\pi \Delta f$$

$$L_2 = R (f_2 - f_1)/4\pi f_1 f_2 = R\Delta f/4\pi f_1 f_2$$

$$C_1 = (f_2 - f_1)/4\pi R f_1 f_2$$

$$C_2 = 1/\pi R (f_2 - f_1)$$

If we require $R = 93\,\Omega$ and $f_2 - f_1 = 100$ kc, then:

Center frequency, mc	$L_1/2$ μhy	L_2 μhy	$2C_1$ pf	C_2 μf	Q
0.5	150	2.99	650	0.034	5
1	"	0.74	180	"	10
2	"	0.18	47	"	20
3	"	0.08	18	"	30

(c) Crystal Filter

Another approach to electrical filtering is to install a commercial (e. g. Bliley, Midland-Wright, etc.) crystal filter. The characteristics of some typical Bliley filters are tabulated in Table 2. (See also figure 17c).

The Q's shown are only approximate. A better calculation would use Δf at the 3 db, not 6 db points, yielding a higher Q. However, it is clear that crystal filters offer Q's one or two orders of magnitude higher than the two simple filters discussed above.

The Q of a crystal filter can be adjusted by changing the output resistor R_2.

Table 2

Characteristics of Crystal Filters

Bliley Elec. Co. Erie, Pa. Type No. BFN-	Center Freq. mc	BW Betw. 6 db Points cps-	BW Betw. 60 db Points kc-	Max. CW Insertion Loss db	$f_0/\Delta f$ = Quality Factor Q
0500 B41	0. 500	300	1. 2	3	1700
2215 B28	2. 215	300	1. 1	1	7500
3000 B14	3. 000	3000	12	3	1000

APPENDIX C

Working Model

1. Equipment

The working model, figure 6, consists of the following commercial equipment:

Arenberg Pulsed Oscillator	PG 650
Arenberg Preamplifier	PA 620B
Lambda Power Supply	Model 28

To generate an analog output proportional to transit time in the gas, a special averaging circuit was designed, constructed and tested.

2. System Characteristics

a. General

In figure 20, at the read-out point, the transit time can be measured as a delay between the arrival of the transmitted pulse (start trigger) and the received pulse, after passage through the gas. Flip-flop V2a, V2b, measures this delay by the time duration that V2a remains conducting. With a 60 cycle repetition rate, meter M1 shows a near full scale deflection for the lowest gas temperature.

b. Detailed Operation of Temperature Read-Out Circuitry

To demonstrate the working model in air, where the attenuation is over 10 times higher than in hydrogen at 5000°R and 600 psia, a convenient low frequency, 500 kc, was chosen. At this frequency, standard IF transformers may be used in the receiving circuit. In general, however, frequencies up to 2 or 3 mc can be used in hydrogen with commercially available equipment.

The pulsed oscillator fires a 500 kc pulse burst, about 25 μsec wide, into crystal A. Simultaneously, a negative gate pulse, 25 μsec

wide, is sent to BNC2. The leading edge triggers V2b to the OFF state (non-conducting) and V2a to the ON state (conducting). Meanwhile, after a time delay depending on the gas temperature, the transmitted pulse burst reaches crystal B where a few millivolts peak to peak are developed by the crystal. A tuned amplifier with 35 db gain increases this pulse signal level to at least 0.5V peak to peak at its output, which is a high impedance point. To eliminate loading effects the next stage is a cathode follower with 100 K input impedance.

At BNC 1 a 0.5V, peak to peak, pulse appears. Cathode follower V1a acts as an impedance transformer, as T1 requires a low source impedance driver due to broadbanding requirements. The desired bandwidth for T1 is about 100 kc between half-power power points, or Q = 5. The measured bandwidth was 110 kc with center frequency of 500 kc. The effective secondary to primary voltage step up ratio is 4:1. After full wave detection, a positive going video pulse, with a 1 mc ripple component, occurs at B. The time constant at point B is adjusted to about one μsec to preserve the pulse rise time. Amplifier V1b has a gain adjustment with sufficient range to insure a pulse of sufficient magnitude to trigger V2a. At point C a negative pulse, 25 μsec wide, with a fast rising leading edge triggers V2a to the OFF state (non-conducting). Then, meter M1 stops passing pulse current. The meter dc current is in the form of a rectangular pulse of fixed amplitude, whose width equals the transit time of 500 kc pulse burst through the gas at any particular temperature. The next oscillator pulse burst causes a repetition of the above cycle. This occurs 60 times a second. As meter M1 reads the average dc value of these pulses, sufficient peak pulse current is passed by V2a to insure that the useful range of M1 is employed. The 5K shunting potentiometer is adjusted for a convenient maximum meter scale reading at the maximum pulse width (maximum delay).

3. Preliminary Calibration

The circuit of figure 20 was designed, constructed and tested. Figure 21 is a plot of meter M1 current versus delay (transit) time through the gas. Transmission through 1 ft of air was achieved. This air path represents typical diameters across which the working model may be expected to operate in laboratory demonstrations.

The electrical output of the integrator has a response time of 1/60 sec at a 60 pps repetition rate. The response time would be 1 msec

at a 1 kc repetition rate. In an actual installation, the sonic thermometer response time can generally be made much less than the limiting response time in the temperature control loop

4. Estimation of Received Signal Level and Signal/Noise Ratio

Based on experiments in room temperature air it is possible to estimate signal levels and S/N ratio in hydrogen at high temperature and pressure.

a. Acoustic Impedance

Figure 11 shows that at the highest temperature and pressure of interest to this contract, the acoustic impedance of hydrogen is four times greater than that of air at NTP. Therefore, ultrasonic energy transmission from a solid probe into high temperature, high pressure hydrogen is 6 db greater than into air[5, 16].

b. Attenuation

At 1 atm, room temperature and 500 kc, the attenuation in air is about 1 db/in., whereas in hydrogen under these conditions the attenuation is about 0.1 db/in.[31]. In hydrogen, when temperature and pressure are increased to their maximum values, 5000°R, 600 psia, the attenuation decreases by an order of magnitude, since the tendency for attenuation to increase at higher temperatures is more than offset by the higher pressure ($\alpha \sim 1/\text{pressure}$). Thus, attenuation in high temperature, high pressure hydrogen is about two orders of magnitude less than in air at NTP. Regarding attenuation, then, measurements over ~1 in. in air near NTP are equivalent to measurements in hydrogen over 1 to 2 ft from NTP up to 5000°R and 600 psia.

c. Beam Spread and Drift

In appendix B2, part d (4), it was stated that beam spread is negligible in the near zone, i.e., within d^2/λ of the transmitter. If one equates the near zone with the nozzle diameter, one can readily calculate the transmitter diameter required to avoid beam spread (e.g., at 500 kc, d = 3 in. for 24 in. hydrogen path). At high gas flow velocity, ~1/10 the sound velocity, the sound beam will be swept downstream (through an angle whose tangent is 1/10, or 6°). If the receiver is axially longer than the transmitter by 1/10 of the nozzle diameter, then a constant fraction of the transmitted pulse will be collected at all flow velocities. If both transmitter and receiver are of equal size, e.g., 3 in. measured axially, then at the highest flow velocities, about 8 db

less signal will be collected, assuming perfect alignment at zero flow. By simply locating the receiver downstream 1 in., the variation in received signal can be kept below 5 db. These numbers are illustrative only. Although 500 kc is used in the working model, an actual system could use frequencies from several hundred kc to 2 or 3 mc. At the higher frequencies, probes could be proportionately smaller (e.g., transmitter dia $\approx$ 1 in. at 3 mc).

From the foregoing paragraphs (a), (b) and (c), it may be concluded that signal levels in hydrogen at high temperature and pressure, across 1 to 2 ft, should be approximately 12 db above signals transmitted across 0.1 in. of air at NTP. In air, using the vane probes of figure 6, 8 mv peak to peak can be generated at the 500 kc receiver crystal. Here, the effective probe area is 0.5 in.^{2}; larger areas would yield proportionately larger signals.

Now in the vibration tests at 500 and 2000 cps to $\pm$ 7g, constant-k filtering reduced the noise below 1 mv. Acoustic isolation and improved filtering can easily reduce this noise even further. Therefore, the expected S/N ratio in hydrogen at 5000°R and 600 psia is better than 10. It may be noted that even when the S/N ratio is <1, the signal can still be retrieved[32]. However, with S/N > 10, elaborate electronic sophistication would not be needed for signal retrieval. A S/N ratio of 10 means the signal is 20 db above the noise.

5. Accuracy

The accuracy of any temperature measurement is ultimately limited by calibration errors. In the laboratory, ultrasonic thermometry of hydrogen up to 5000°R and 600 psia can be accomplished by an absolute accuracy of better than 1/2% (appendix A1; figure 5). The precision of these ultrasonic measurements can be better than 0.1%[3,4].

In flight, the ultrasonic system can measure average gas temperature within 2%. Accuracy is highest at high frequency ($\sim$3 mc) and high repetition rate ($\sim$100 to 1000 pps). This estimate is arrived at as follows:

Based on information available at this time it appears that most of the uncertainties or errors associated with an ultrasonic sensor installed in a particular nuclear rocket nozzle can be kept below 0.1%. For example, if the probe separation is known to 0.020 in. for a 2 ft

gas path, the uncertainty in distance is $< 0.1\%$. Regarding errors associated with the gas, we noted (appendix A4) that if the amount of contaminant is $< 0.1\%$, the error in velocity is also $< 0.1\%$. The boundary layer across the probes produces a smearing of $<< 0.1\%$ (appendix A3). The boundary layer between nozzle walls at $2500^{\circ}R$ and 800 ft/sec hydrogen at $5000^{\circ}R$ should be quite small, but if necessary it could be pierced by protruding probes to eliminate its effect on transit time. The effect of gas flow components parallel and antiparallel to the sound propagation can be estimated to $< 0.1\%$ (appendix A2).

There are possible errors associated with the probes and waveguides (if required). Radiation effects on sound velocity are negligibly small in some materials[13]. Temperature gradients from $30^{\circ}R$ to $2500^{\circ}R$ cause a corresponding sound velocity gradient. However, both radiation effects, if they exist, and temperature gradients, can be compensated for by incorporating a simple pulse echo measurement into the sensor system, so that the transit time in probes and waveguides is subtracted from the total transit time.

Electronic errors consist of jitter at the transmitter, and variation in multivibrator switching on and switching off times. With a bootstrap circuit to sharpen trigger pulses, turn on and turn off times can be shortened until the probable error is 0.15% for any particular pulse. Since the temperature control loop averages over many pulses even in 0.1 sec, the errors due to turn on and turn off time variations can be made negligibly small, $<< 0.1\%$.

The largest electronic error appears due to uncertainty in detecting the average time of arrival of the pulse after passage through the gas. The pulse builds up gradually, taking on the order of 10 cycles to reach a maximum at the receiver crystal of about 10 mv peak to peak, with S/N>10. When the pulse amplitude reaches a predetermined level, the multi is turned off, stopping the integration for that pulse. Now, if turbulence or other random variables cause the signal to jitter in amplitude, the multi may be erroneously turned off one or more cycles too soon or too late. To minimize this time of arrival error, high frequency, ~3 mc, and high repetition rate, are recommended. For example, at 3 mc, the error in temperature due to "missing" 1 cycle is 0.4% at $5000^{\circ}R$. If more than one cycle is "missed," the error in measuring the time of arrival of that particular pulse would be proportionately larger. It is important to note, however, that in a sampling time of 0.1 sec, at a 1 kc

repetition rate, 100 pulses would be detected and their transit times averaged. If the measured transit times are distributed above and below the true transit time due to random effects in the ultrasonic path, then the errors in arrival time tend to cancel one another, and the measured average temperature would closely approach the average temperature.

Based on the above analysis, admittedly simplified, it is concluded that in particular installations, the ultrasonic sensor could measure average exhaust gas temperature in a nuclear rocket engine within 2%.

VII. ACKNOWLEDGMENT

The authors gratefully acknowledge the cooperation of the staff of the MIT research reactor, especially A. Arena, L. R. Enstice, D. Frech and G. Woodruff. The radiation tests were also guided in part by Prof. R. Truell. Most of the experiments were conducted by B. R. Douglass. B. Sellers performed the calculations in appendix B1. R. Kyracou designed the integrator and read-out circuit. Construction of the high temperature, high pressure furnace was substantially aided by the cooperation of C. D. Pears, F. Digesu and J. Woodward of the Southern Research Institute.

VIII. REFERENCES

1. G. P. Sutton, Rocket Propulsion Elements, 3rd Ed., Wiley, New York, p. 452, (1963).

2. E. H. Carnevale, H. Poss, and J. Yos, "Ultrasonic Temperature Determinations in a Plasma." Temperature - Its Measurement and Control in Science and Industry, Vol. 3, Part 2, 959 (1962).

3. E. H. Carnevale, G. S. Larson, and L. C. Lynnworth, Abstract F7 in J. Acoust. Soc. Am. 35, 1883, Nov. 1963.

4. E. H. Carnevale, G. S. Larson and L. C. Lynnworth, Ultrasonic Transport Property Measurements in High Temperature Gases, presented at the APS Div. of Fluid Dynamics Meeting, Pasadena, Calif. (Nov. 23-25, 1964).

5. G. S. Larson, R. N. Lawson, and L. C. Lynnworth, Upper Atmospheric Sonic Thermometry, presented at ISA-AMS Joint Session, Atmospheric Temperature Measurement, 19th Annual ISA Conference, New York City (Oct. 12-15, 1964); ISA Preprint No. 19. 1-5-64.

6. A. M. Mayer, Phil. Mag., 45, 18 (1873).

7. C. G. Suits, Physics, 6, 190 (1935).

8. J. Livengood, T. Roma, and J. Baruch, J. Acoust. Soc. 26, 824 (1954).

9. F. R. Gilmore, "Equilibrium Composition and Thermodynamic Properties of Air to 24,000°K, RM-1543, August 1955, Rand Corp., Santa Monica, Calif.

10. National Bureau of Standards, Tables of Thermal Properties, pp. 75-137, Circular 564, (November 1955).

11. Ibid., pp. 254-296 (Ref. 6); N. T. Grier, NASA TN D-1406, Calculation of Transport Properties and Heat-Transfer Parameters of Dissociating Hydrogen (Oct. 1962).

REFERENCES (cont'd)

12. K. R. Herzfeld and T. A. Litovitz, Absorption and Dispersion of Ultrasonic Waves, Academic Press, New York (1959).

13. R. Truell, Metals Research Laboratory, Brown University, private communication; R. Truell, J. Teutonico and P. W. Levy, Phys. Rev. 105, 1723-1729 (15 Mar. 1957); R. Truell, Phys. Rev. 116, 890-892 (15 Nov. 1959).

14. Sources of data: C. H. Hodgman, R. C. Weast, and S. M. Selby. Handbook of Chem. and Phys., Chem. Rubber Publ. Co., Cleveland (1956), 2043, 2130. Dow-Corning brochure, Form No. 11-011. (1963).

15. MIT's research reactor is currently operated at 2 Mw. There are other reactors in the U. S. with flux levels greater by 1 or 2 orders of magnitude. See, for example, D. J. Hamman and W. H. Veazie, Jr., Survey of Irradiation Facilities, REIC Rept. No. 31 (Part I) to ASD, AFSC (Sept. 15, 1963).

16. L. C. Lynnworth, Ultrasonic Impedance Matching from Solids to Gases, presented at 68th Meeting, Acoust. Soc. Amer., Austin, Texas (Oct. 22, 1964); abstract in J. Acoust. Soc. Amer. 36 (10), 1999 (Oct. 1964); IEEE Trans. Sonics and Ultrasonics SU-12 (2) (1965).

17. K. Eldred, Wyle Laboratories, Huntsville, Ala., private communication at 67th Meeting, Acoustical Society of America, New York City, (May, 1964).

18. R. N. Tedrick, J. Acoust. Soc. Amer. 36, 2027-2032 (Nov. 1964).

19. F. M. Weiner, "Rocket Noise of Large Space Vehicles," in Proc. 4th Int. Congress on Acoust., Copenhagen, 1962. (Org. Comm. of the 4th ICA and Harlag & Toksvig, Copenhagen, 1962), Pt. 2, p. 231.

20. T. J. B. Smith and J. K. Kilham, J. Acoust. Soc. Amer. 35, 715-724 (1963).

21. J. K. Manhart, Douglas Missile and Space System Div., private communication, (29 Oct. 1964); Prog. Rpt., KIWI B Acoustical Study (Oct. 1964).

22. C. D. Pears, A Progress Report on a 6500°F Furnace for Thermophysical Property Studies, presented at the Thermal Cond. Conf. Gatlinburg, Tenn., (Oct. 1963); C. D. Pears, F. J. Digesu and J. D. Woodward, The True Stress-Strain Properties of Brittle Materials to Very High Temperatures, Final Rpt. to AEC, 1963-1964, under contract No. AT-(40-1) - 2694 (Oct. 30, 1964); Research/Development 15 (8), cover, 9 (Aug. 1964).

23. H. Schlichting, Boundary Layer Theory, 4th Ed., McGraw-Hill, N. Y., p. 647 (1960).

24. G. Woodruff, Master's Thesis, MIT (Jan. 1963); Ph. D. thesis, MIT (to be published); private communication (16 April 1964).

25. G. P. Sutton, op. cit., p. 404.

26. T. F. Hueter and R. H. Bolt, Sonics, Wiley, New York (1955), pp. 61-66.

27. F. E. Terman, Electronic and Radio Engineering, 48, McGraw-Hill, New York (1955).

28. W. L. Everitt and G. E. Anner, 249-293, Communication Engineering, McGraw-Hill, New York (1956).

29. E. H. Carnevale, L. C. Lynnworth and G. S. Larson, J. Acoust. Soc. Amer. 35 (11), 1883 (Nov. 1963); 36 (9), 1678-1684 (Sept. 1964); 36 (10), 1999 (Oct. 1964).

30. Young's modulus in aluminum alloys, from 140 to 1060°R, is plotted in Mil Handbook 5, p. 3. 2. 6. 2. 5. (a) (6061) and p. 3. 2. 7. 1. 4 (7075)(Aug. 1962); ref. 29 gives Young's and shear moduli and Poisson's ratio in 6061 from 530 to 1550°R; E. G. Stanford, Nuovo Cimento, Suppl. A1 Vol. VII, Series IX (No. 2), 332-340 gives Young's modulus in 99.992% from 530 to 1650°R. For tungsten, B. T. Bernstein, J. Appl. Phys. 33 (6), 2140 (June, 1962) gives shear wave velocities from 530 to 2350°R, and longitudinal wave velocities from 530 to 3730°R. DMIC Rpt. 191 (Sept. 27, 1963), p. A-30 gives Young's modulus in W from 530 to 5360°R.

REFERENCES (cont'd)

31. J. J. Markham, R. T. Beyer and R. B. Lindsay, Rev. Mod. Phys. 23, (4), 391, 353-411 (Oct. 1951).

32. Princeton Applied Research Corp., Electronic Design 12 (24), 70 (Nov. 23, 1964).

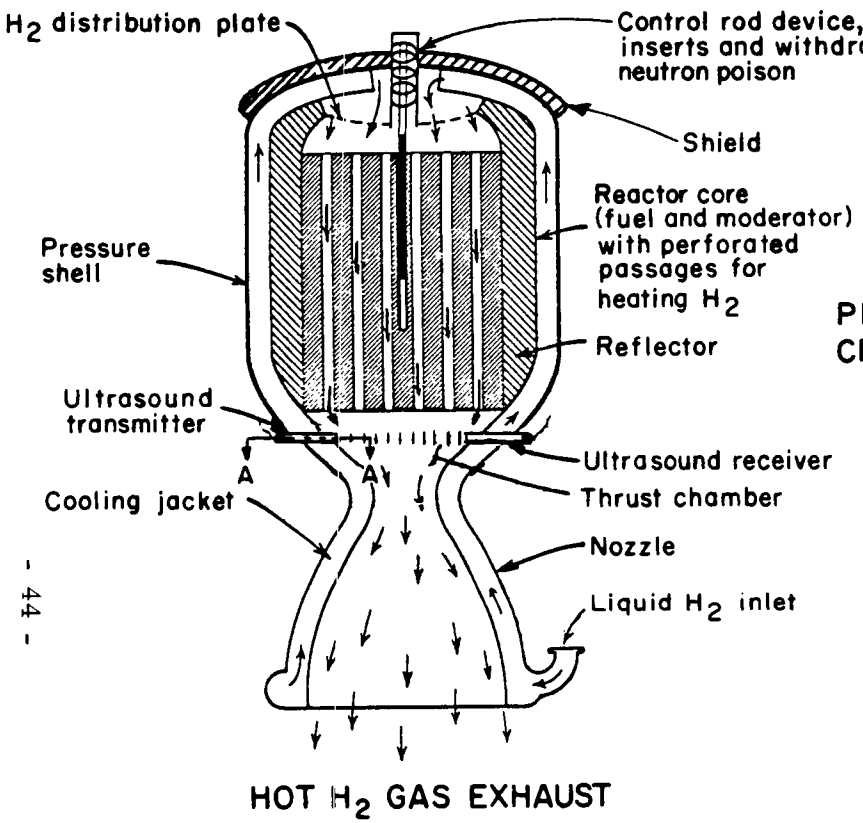

Figure 1a. Schematic diagram of fission reactor for nuclear rocket shows measurement location of ultrasonic temperature sensor (diagram adapted in part from Sutton[1], p. 390).

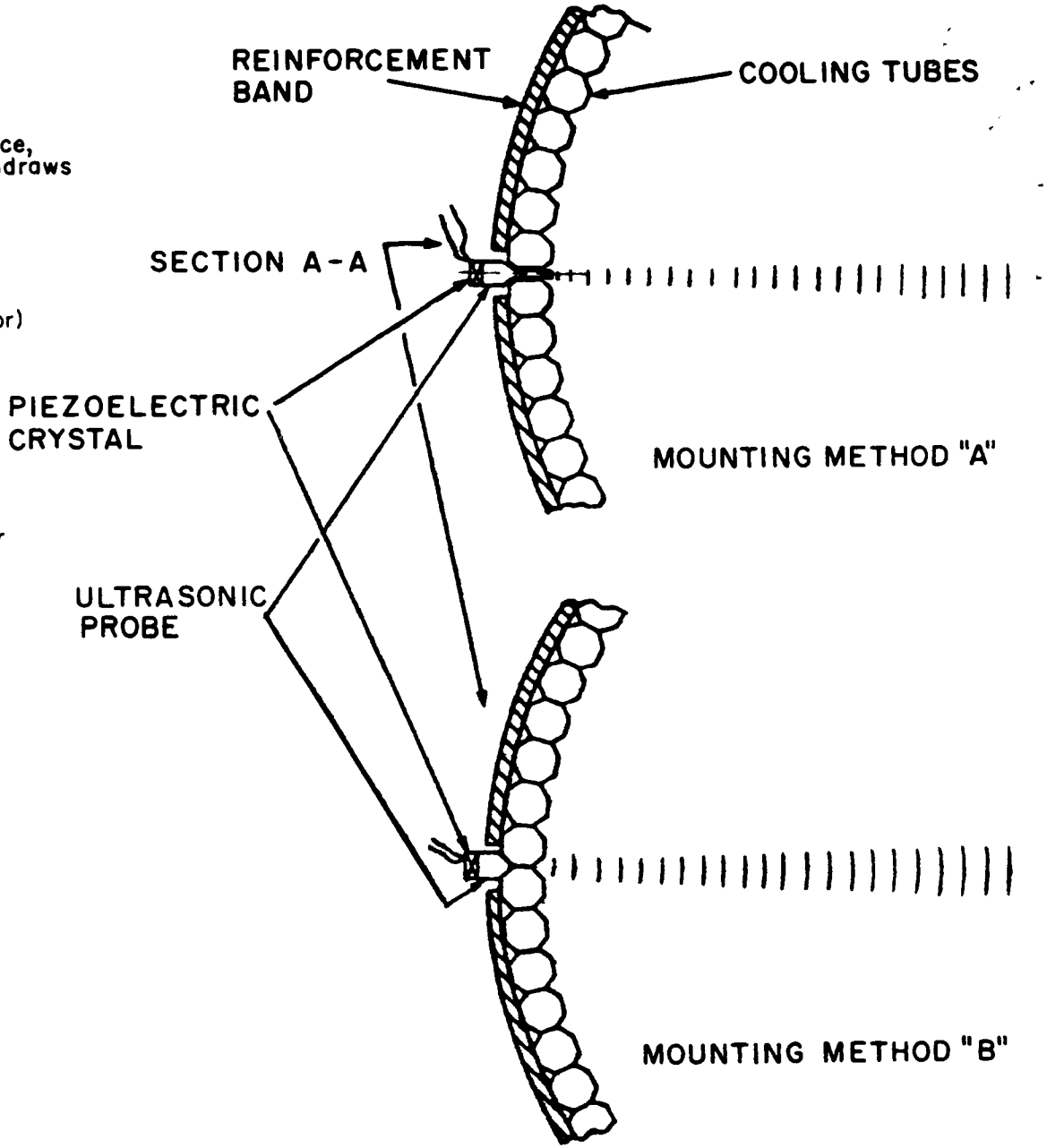

Figure 1b. Mounting methods. Mounting method "A" employs concept of inserting ultrasonic sensing probe between cooling tubes of thrust chamber, thereby allowing probe to protrude into the interior of thrust chamber. Mounting method "B" employs concept of mounting probe on exterior of thrust chamber, but in intimate contact with cooling tubes or reinforcement band.

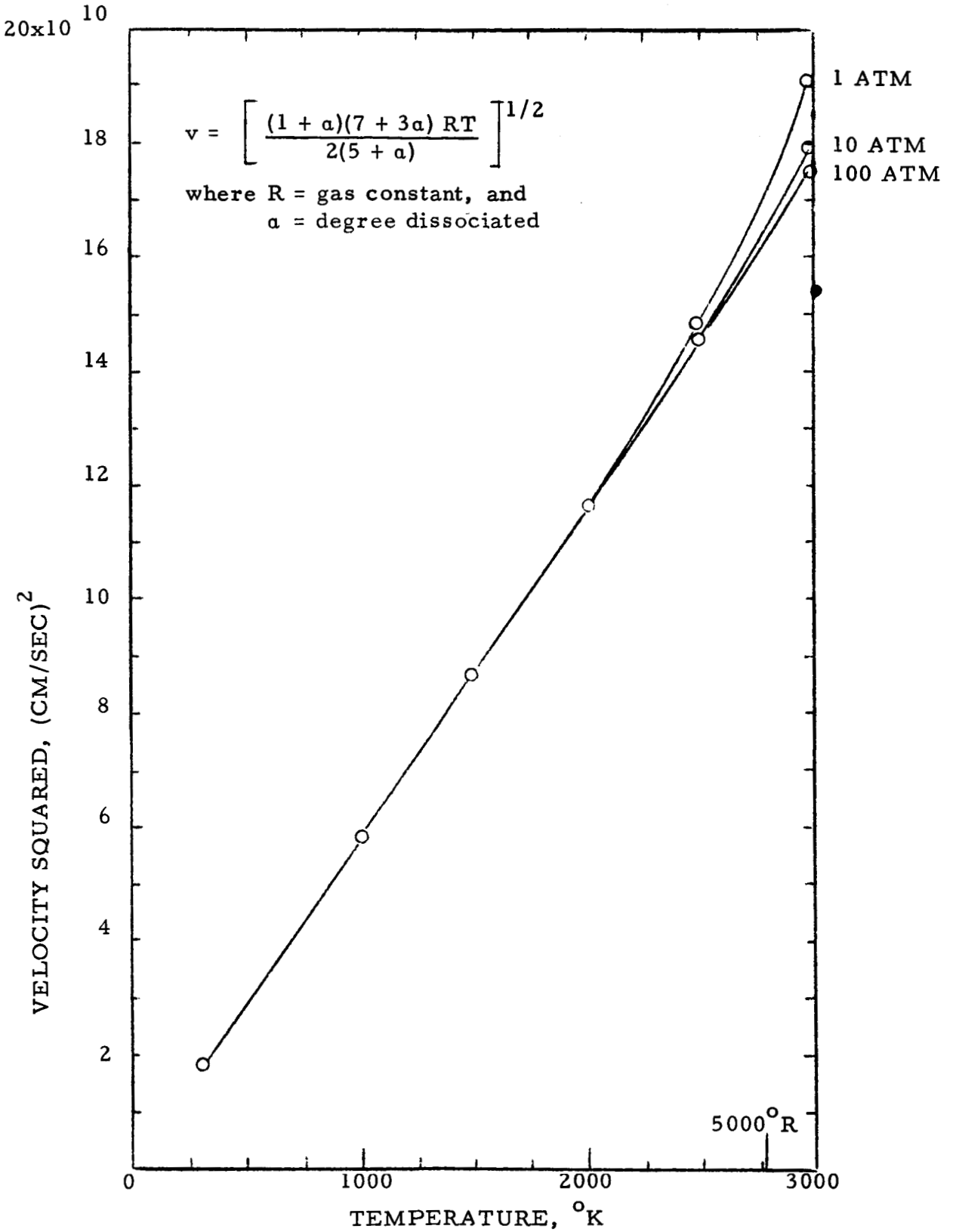

Figure 2. VELOCITY SQUARED VS. TEMPERATURE IN HYDROGEN

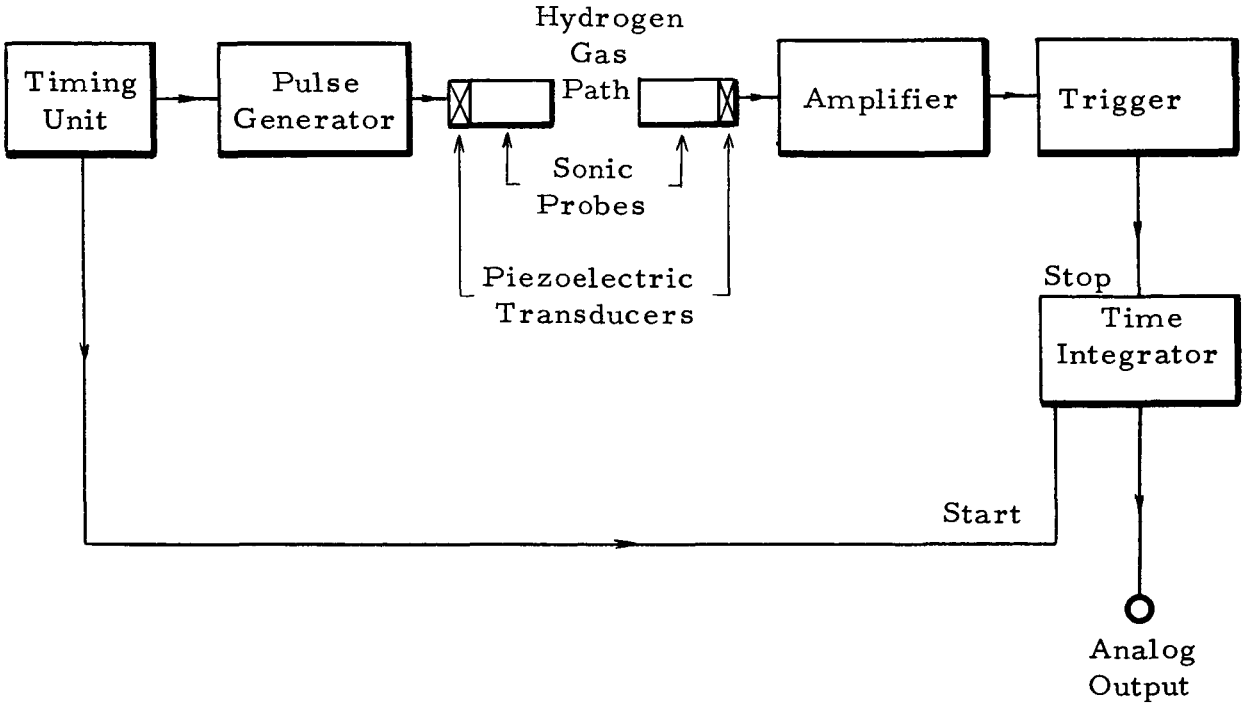

Figure 3. BLOCK DIAGRAM OF THERMOMETRY SYSTEM USING ULTRASONIC PULSE TECHNIQUE.

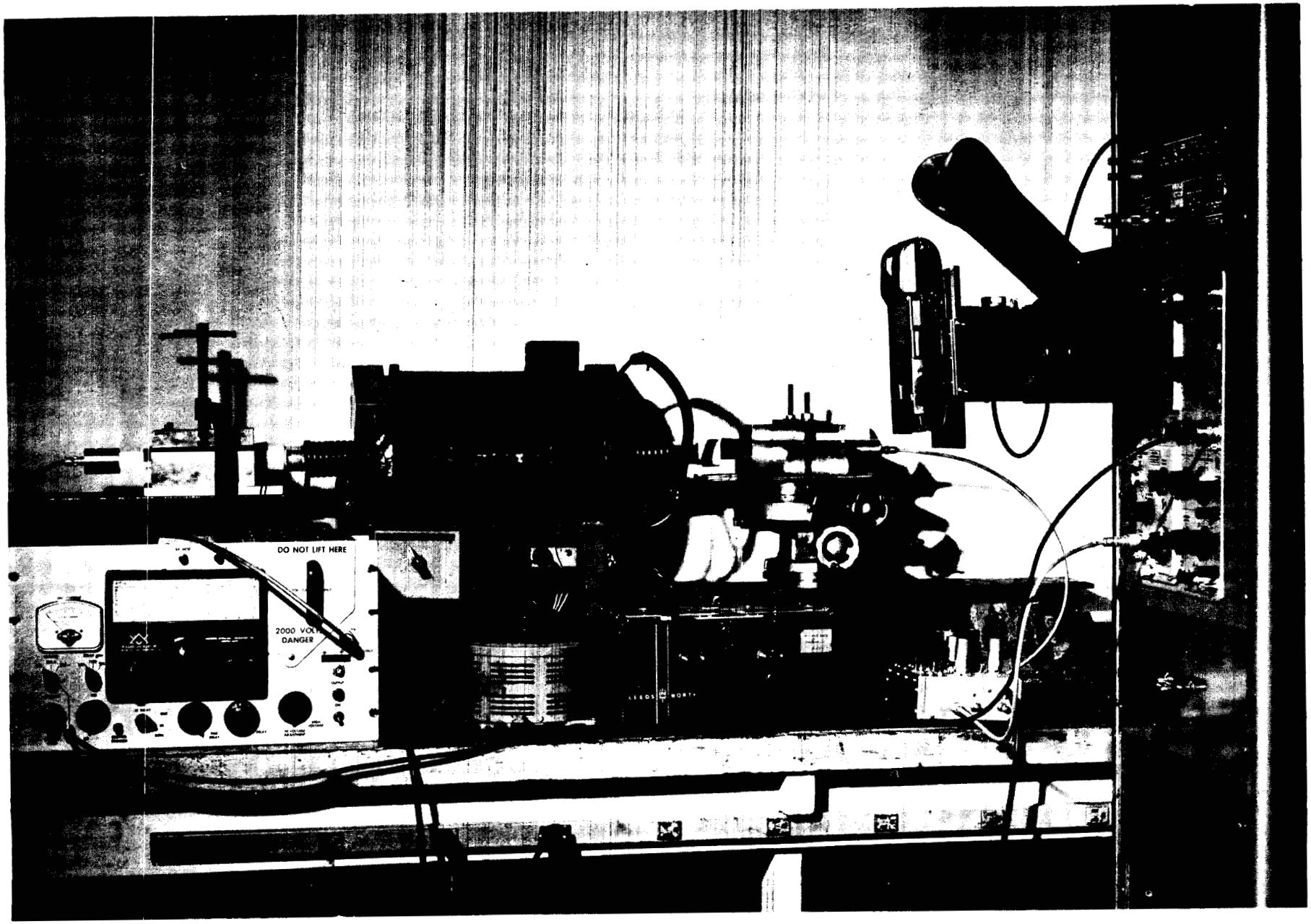

Figure 4. 2300°R MUFFLE TUBE

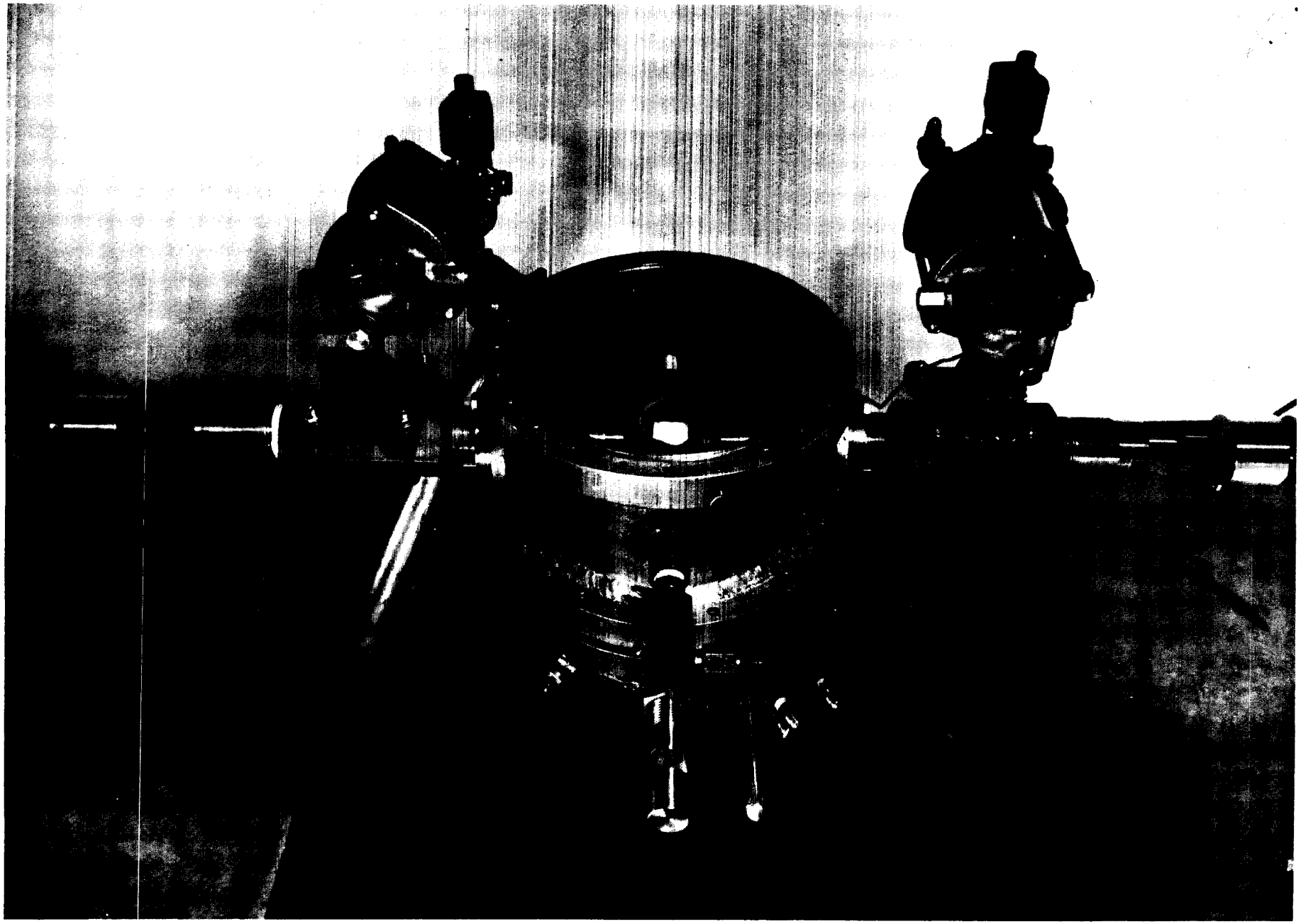

Figure 5. ULTRASONIC PROBES ABOUT TO ENTER HOT ZONE IN HIGH TEMPERATURE, HIGH PRESSURE OVEN

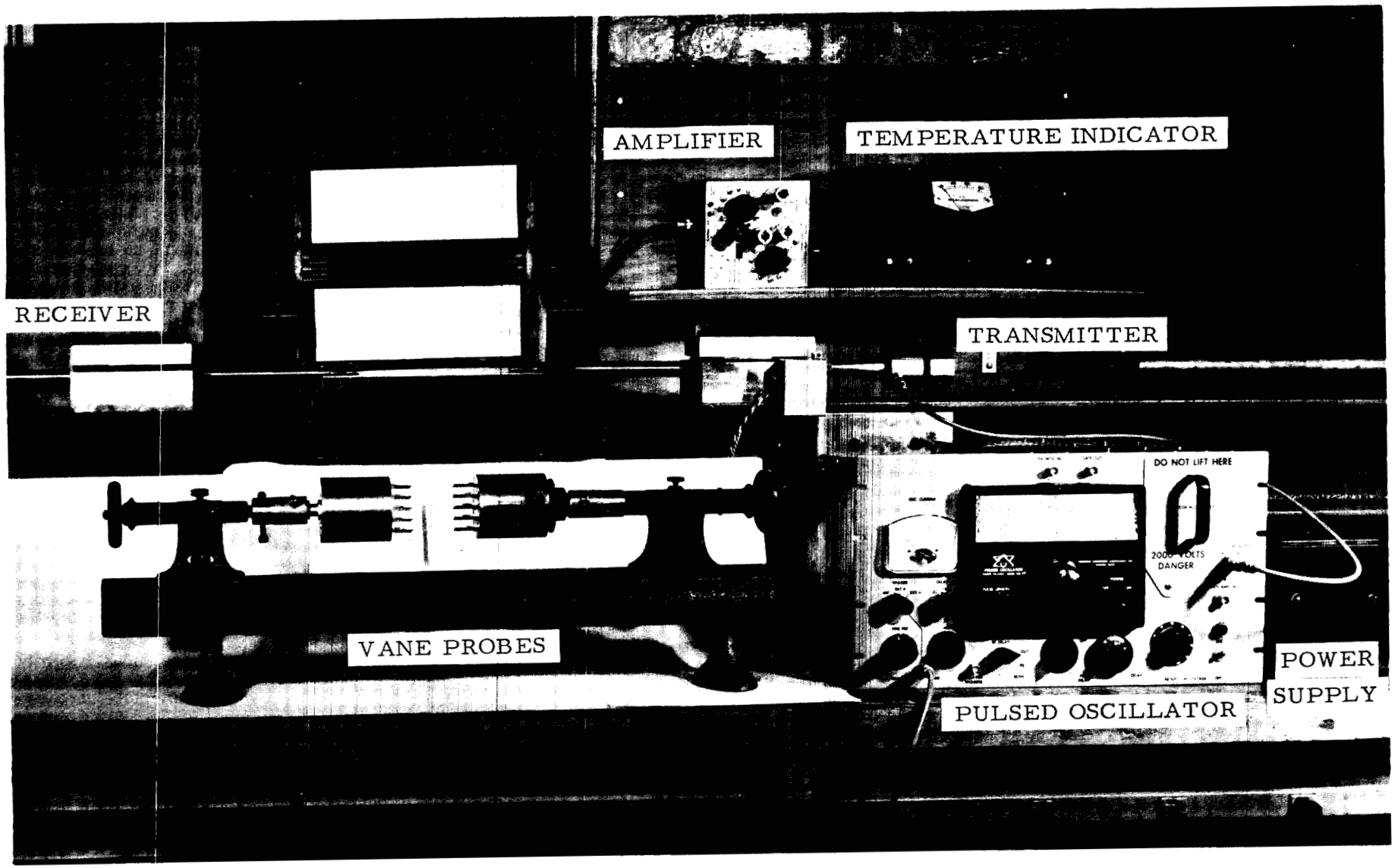

Figure 6. WORKING MODEL OF ULTRASONIC THERMOMETER

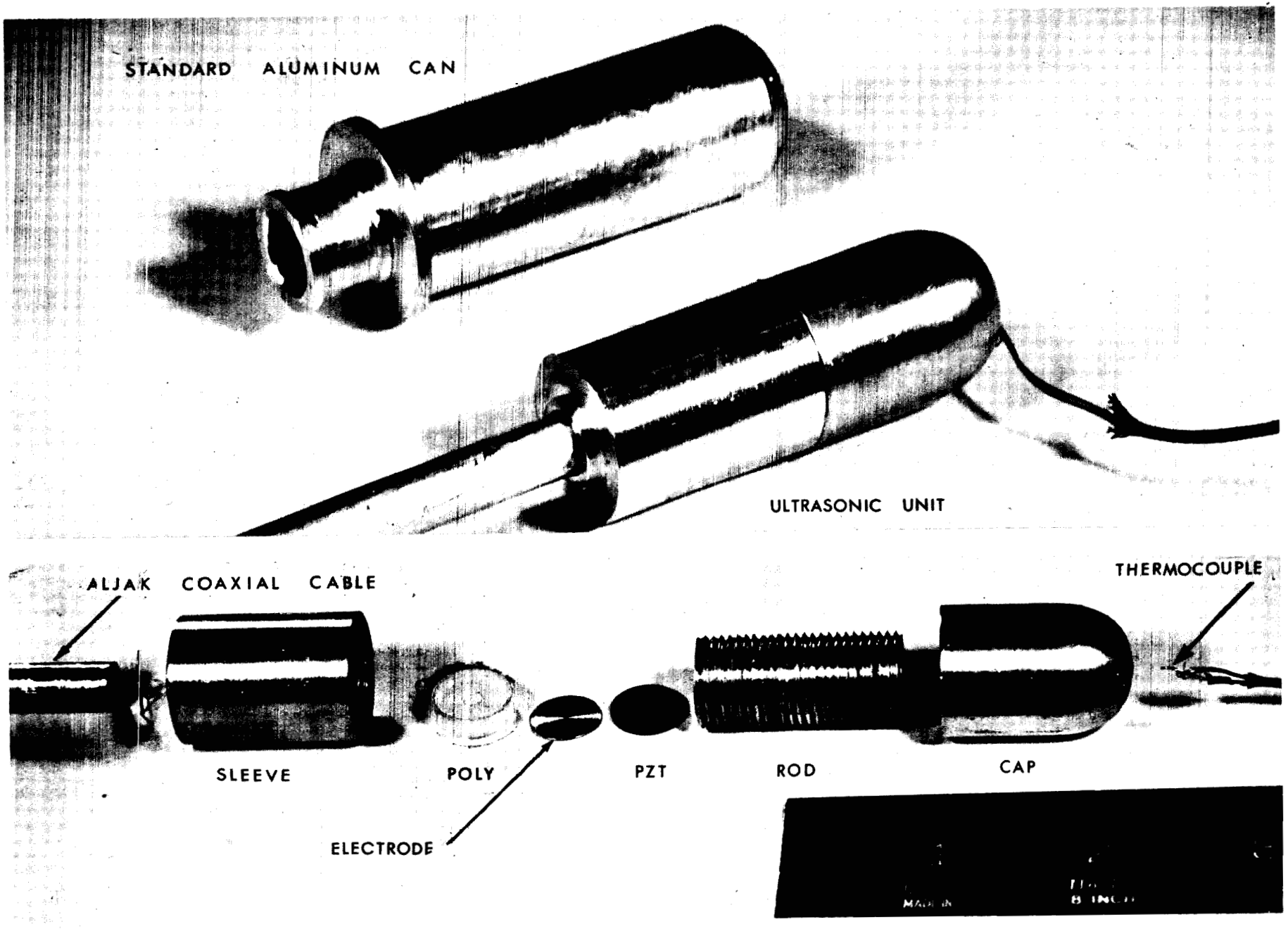

Figure 7. ULTRASONIC UNIT FOR RADIATION TEST

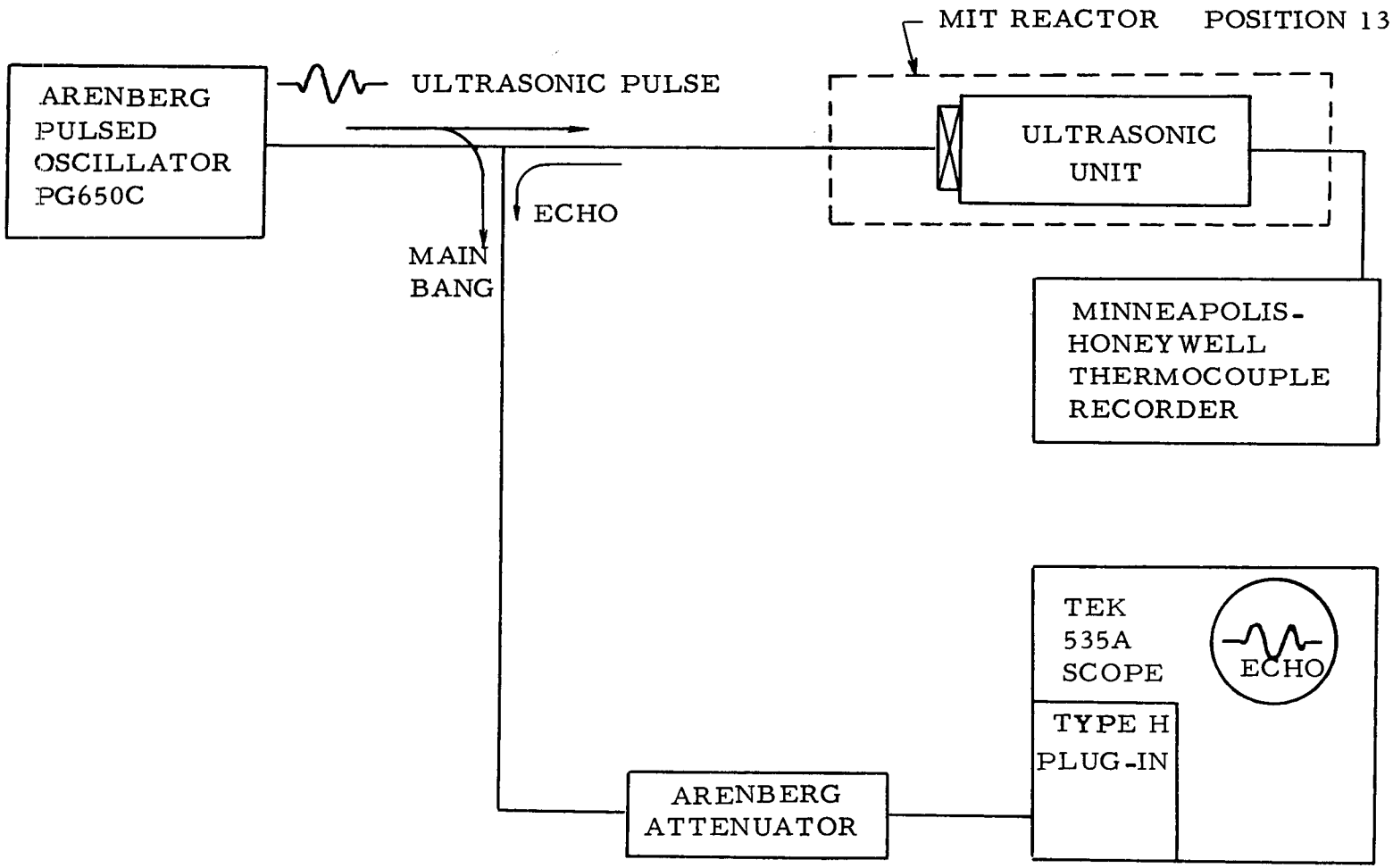

Figure 8. IRRADIATION EXPERIMENT BLOCK DIAGRAM

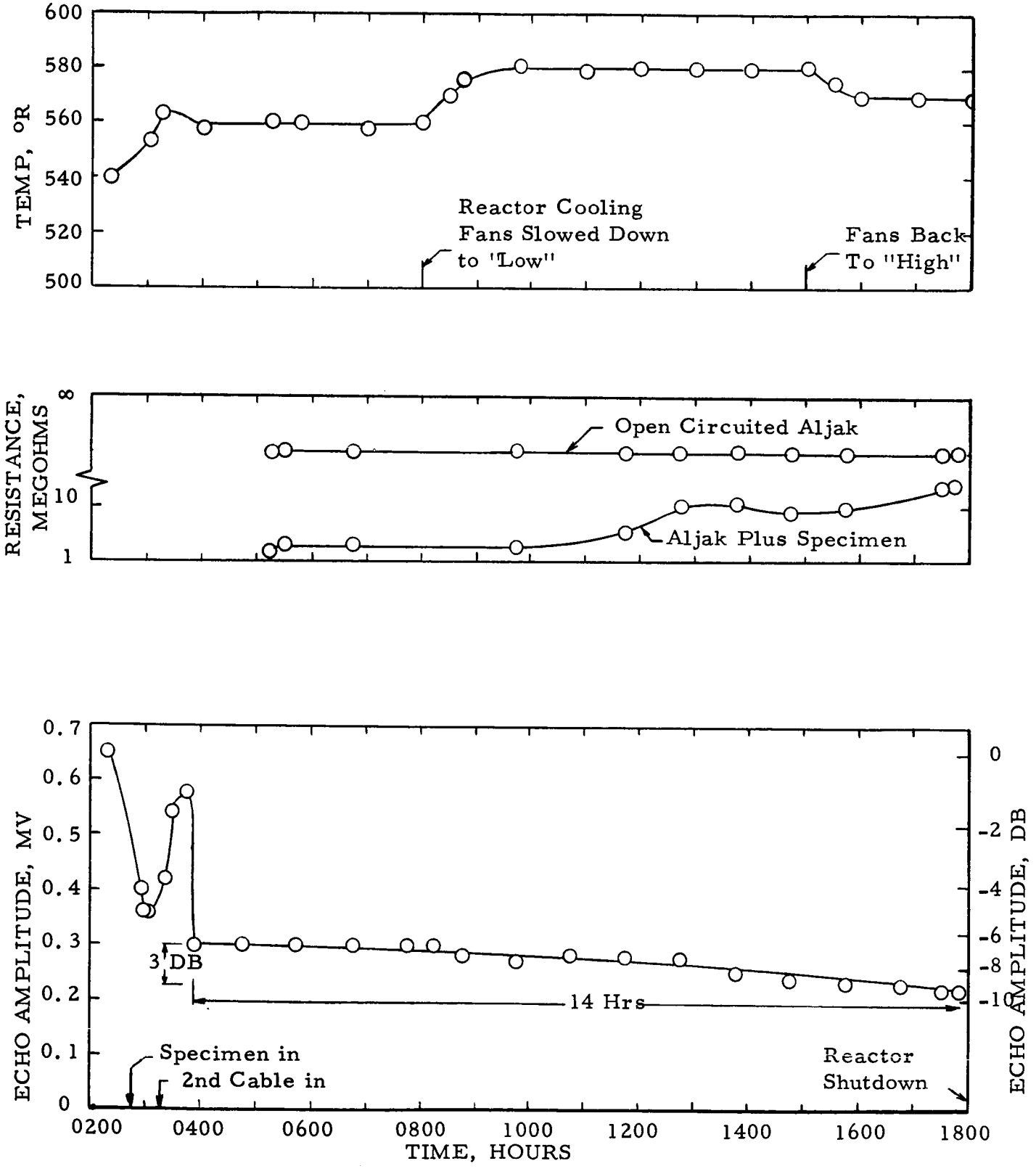

Figure 9. TEMPERATURE, RESISTANCE AND ECHO AMPLITUDE VS. TIME
(Test conducted in MIT nuclear reactor on 3 April 1964, 2 am to 6 pm)

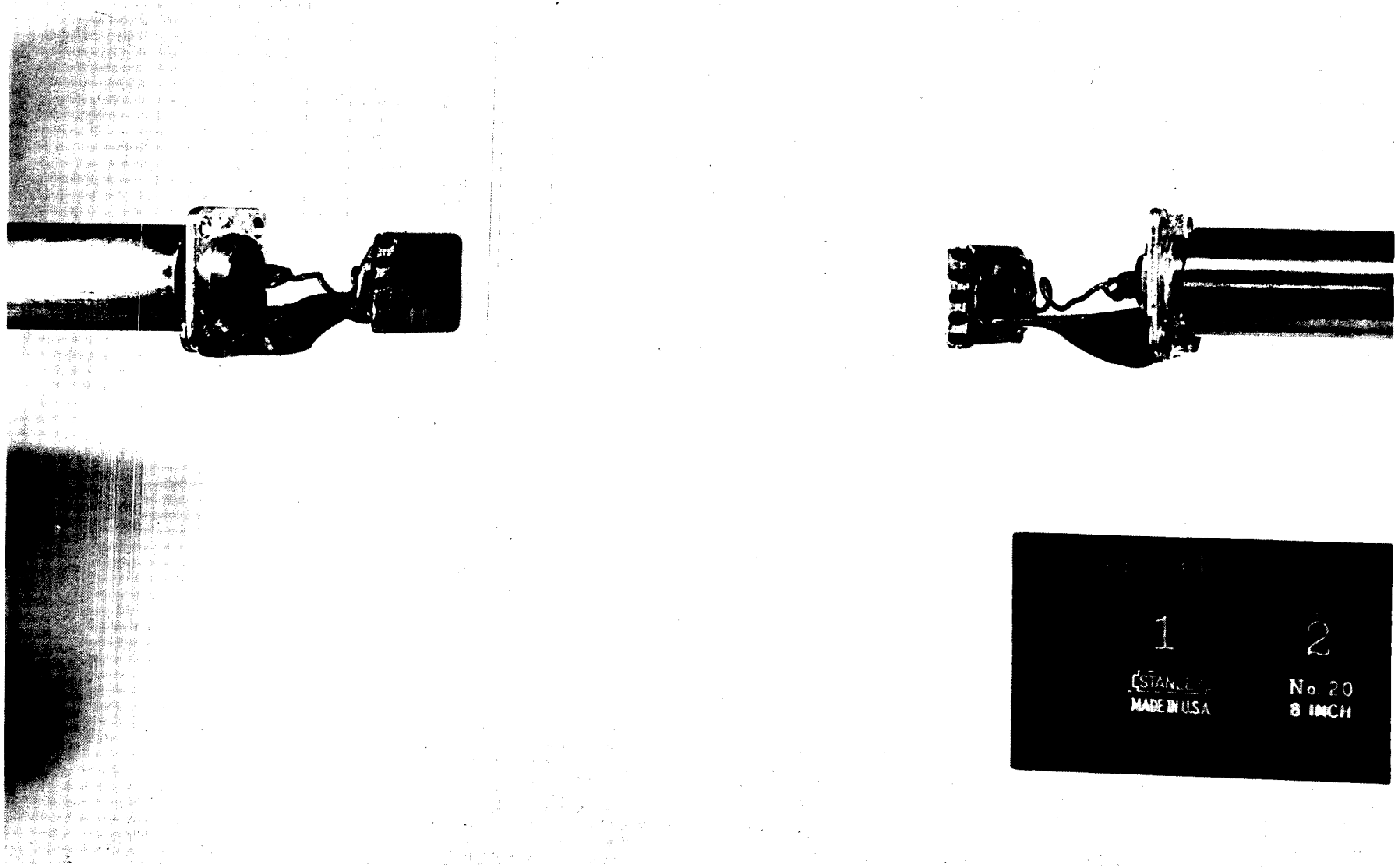

Figure 10. ULTRASONIC TRANSMISSION THROUGH BRAZED TUBING

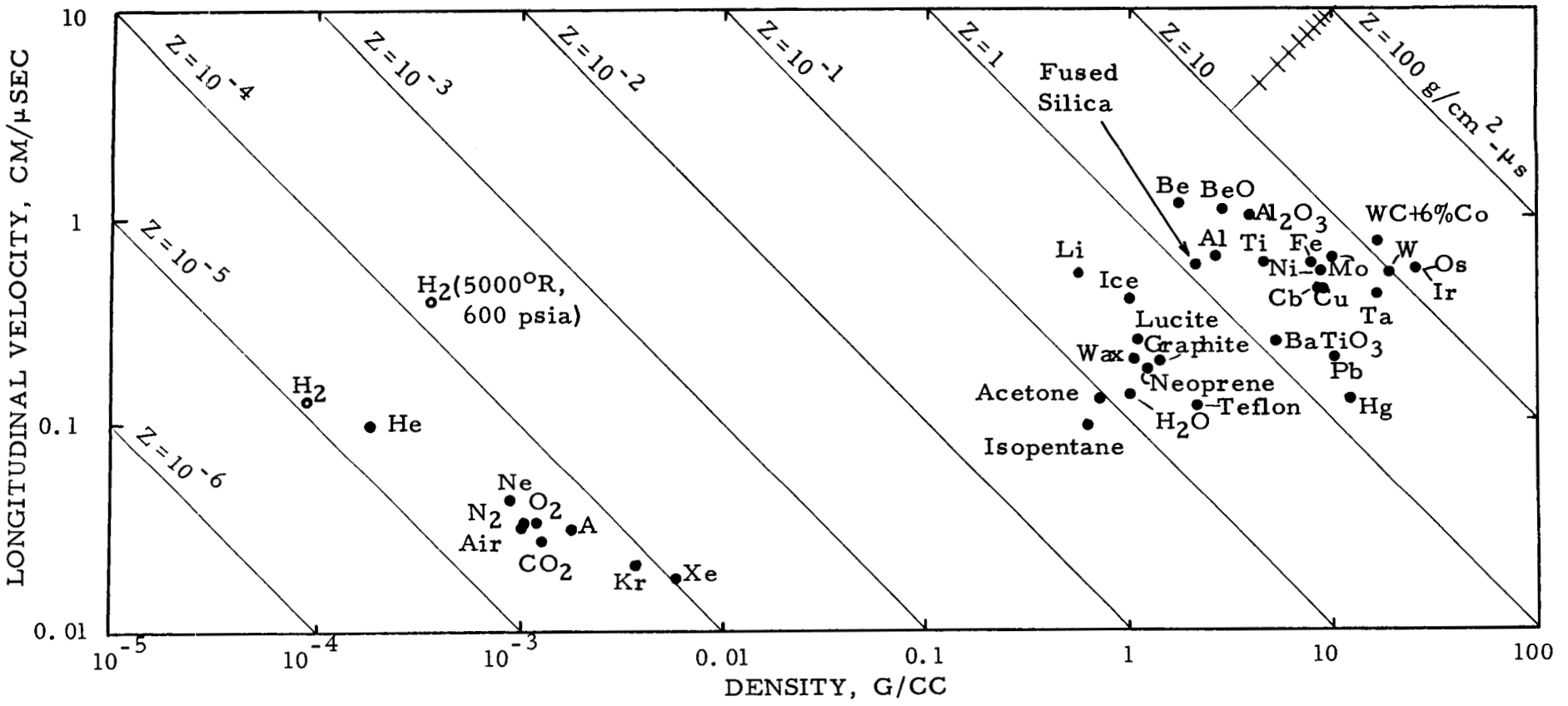

Figure 11. LONGITUDINAL WAVE ACOUSTIC IMPEDANCE NOMOGRAM CATALOGUES MATERIALS IN TERMS OF DENSITY AND LONGITUDINAL WAVE VELOCITY. LINES AT 45° ARE LINES OF CONSTANT LONGITUDINAL WAVE ACOUSTIC IMPEDANCE.[5, 16]

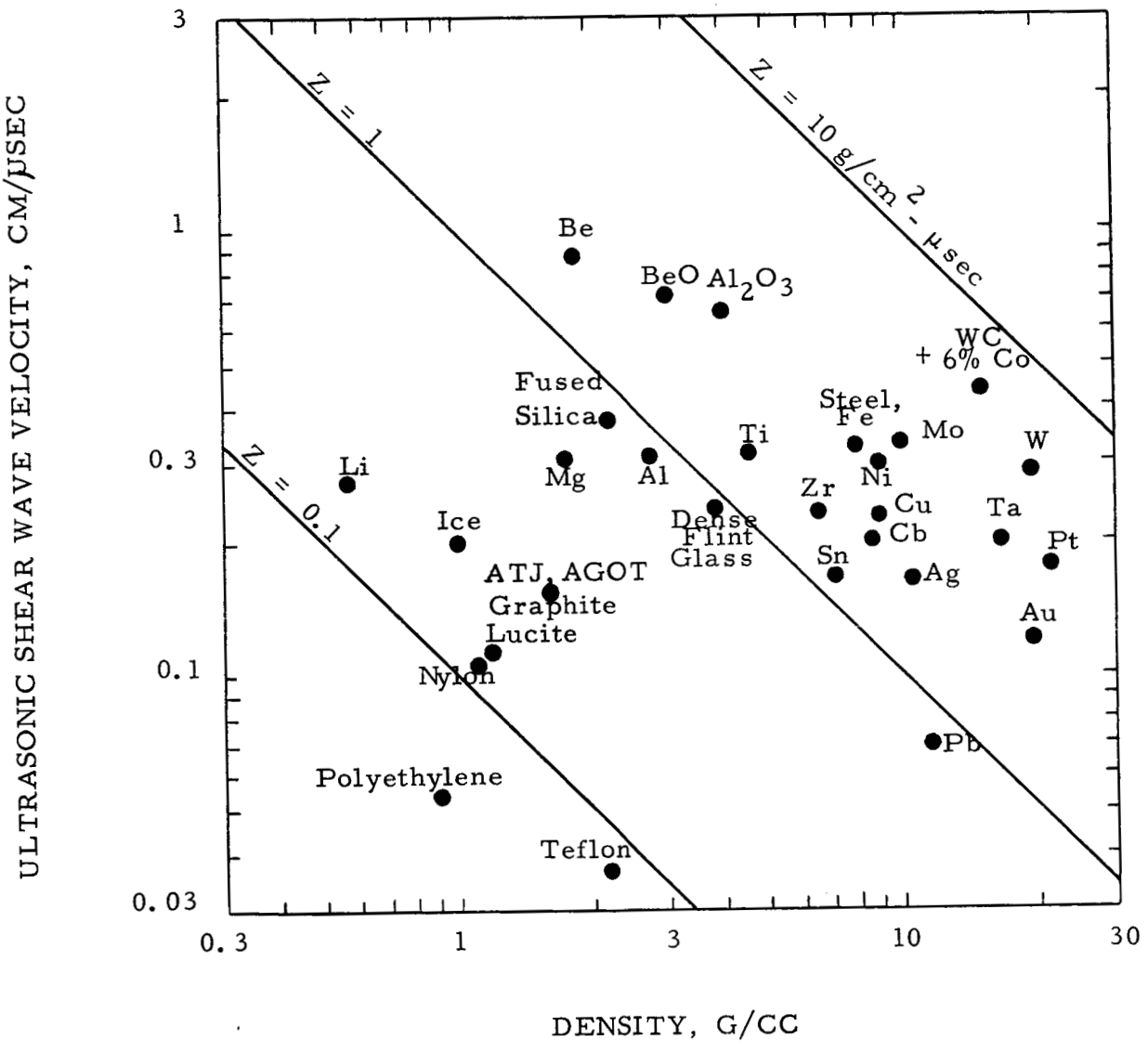

Figure 12. SHEAR WAVE ACOUSTIC IMPEDANCE NOMOGRAM CATALOGS SOLIDS IN TERMS OF ULTRASONIC SHEAR WAVE VELOCITY AND DENSITY. LINES AT 45° ARE LINES OF CONSTANT ACOUSTIC SHEAR WAVE IMPEDANCE.

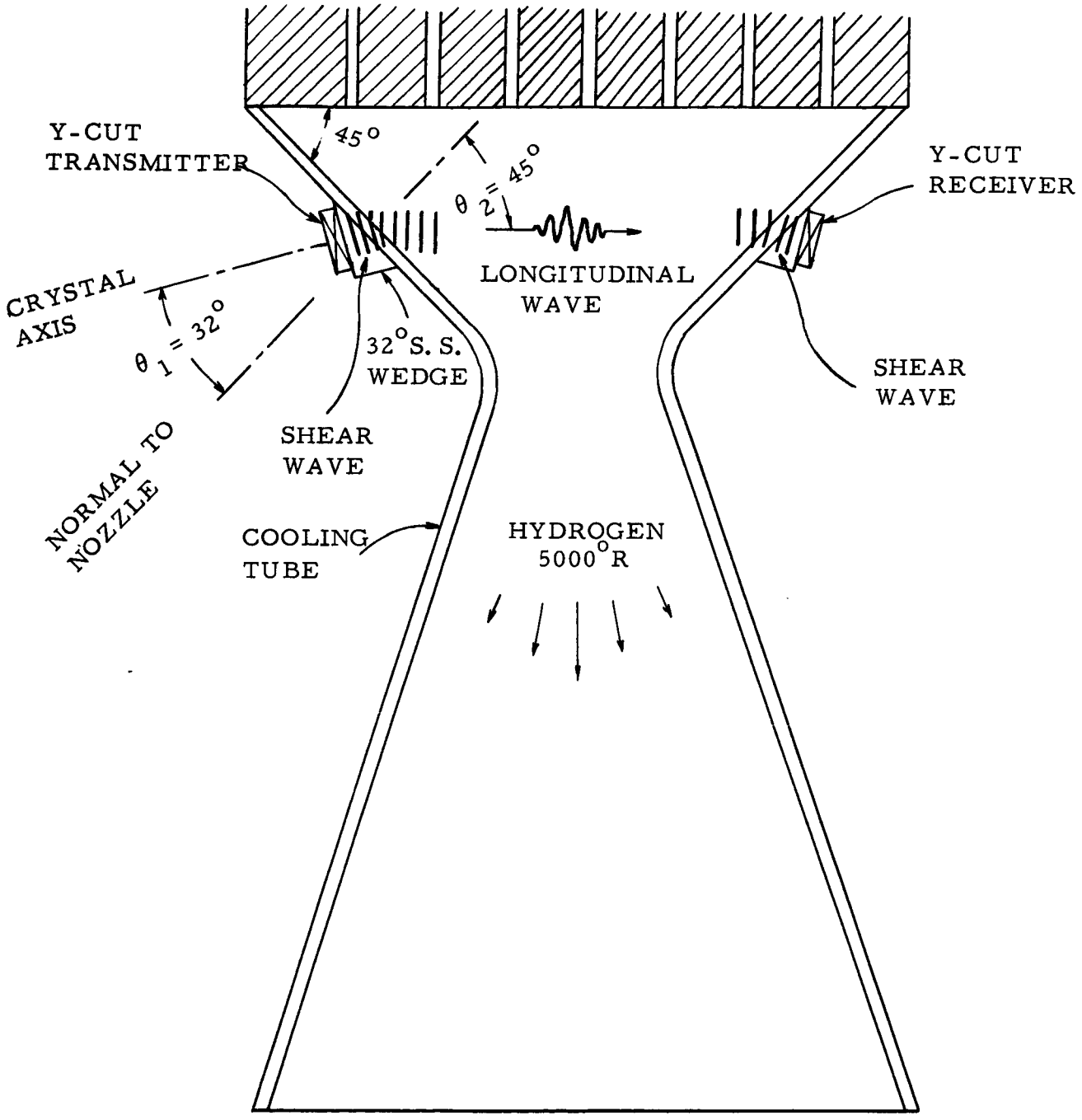

Figure 13. REFRACTION AND MODE CONVERSION OF SHEAR WAVE INTO LONGITUDINAL WAVE AT TRANSMITTER, AND BACK TO SHEAR WAVE, AT RECEIVER.

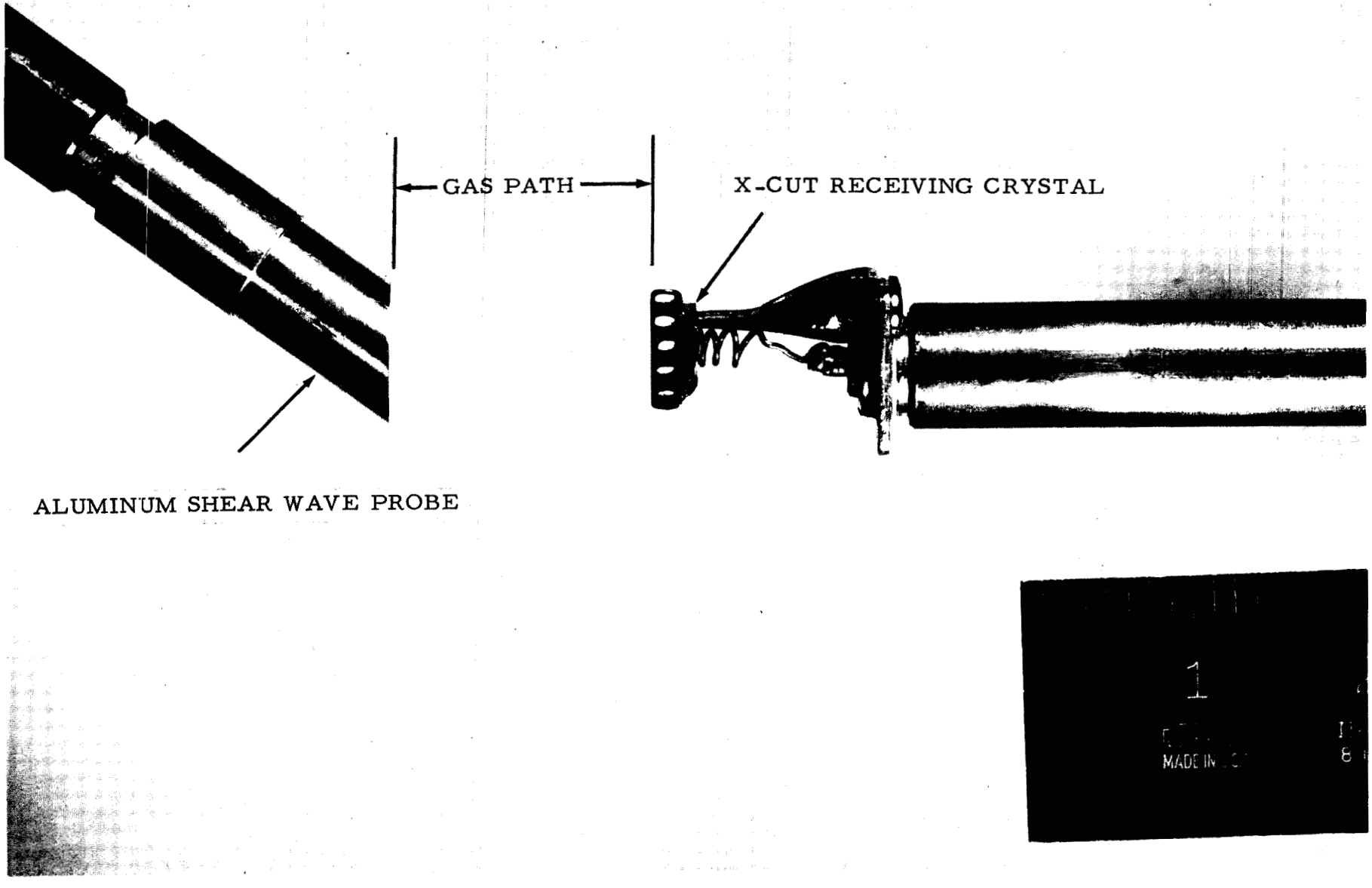

Figure 14. SHEAR WAVE IN ALUMINUM PROBE CONVERTED TO LONGITUDINAL WAVE IN GAS

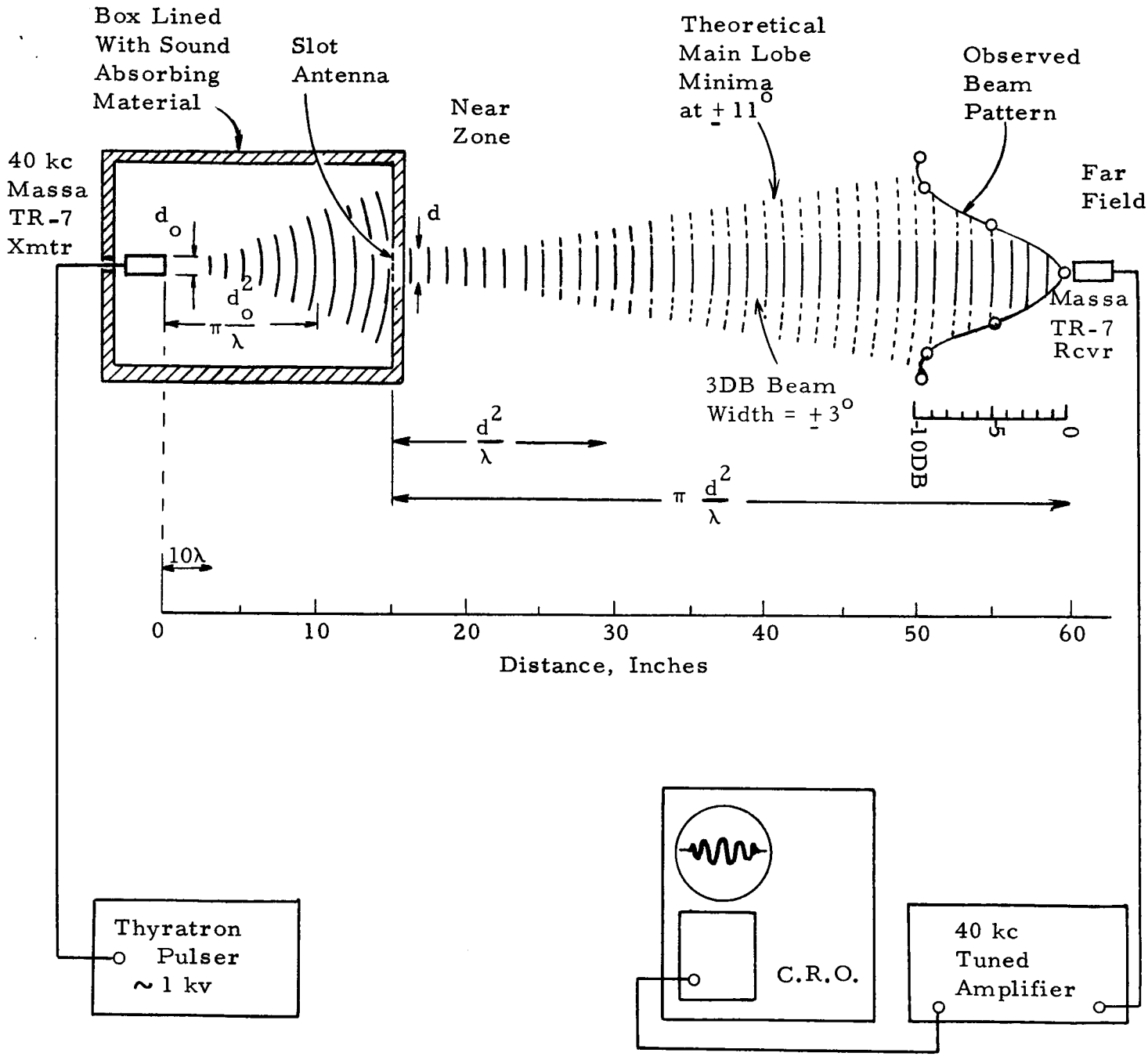

Figure 15. SCHEMATIC DIAGRAM OF 40 KC SCALED EXPERIMENT IN AIR, AND OBSERVED BEAM PATTERN.

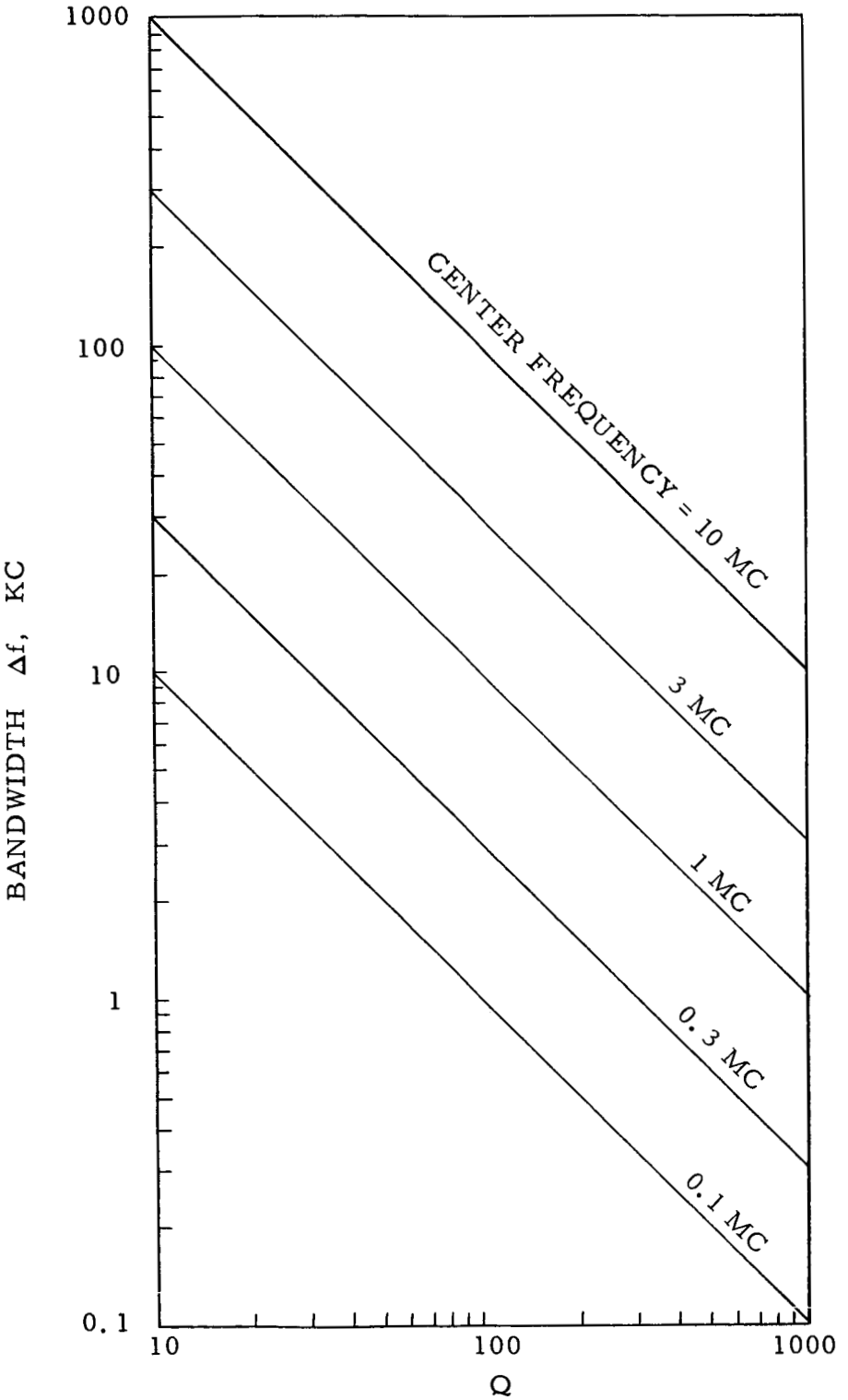

Figure 16. BANDWIDTH VS Q AND CENTER FREQUENCY

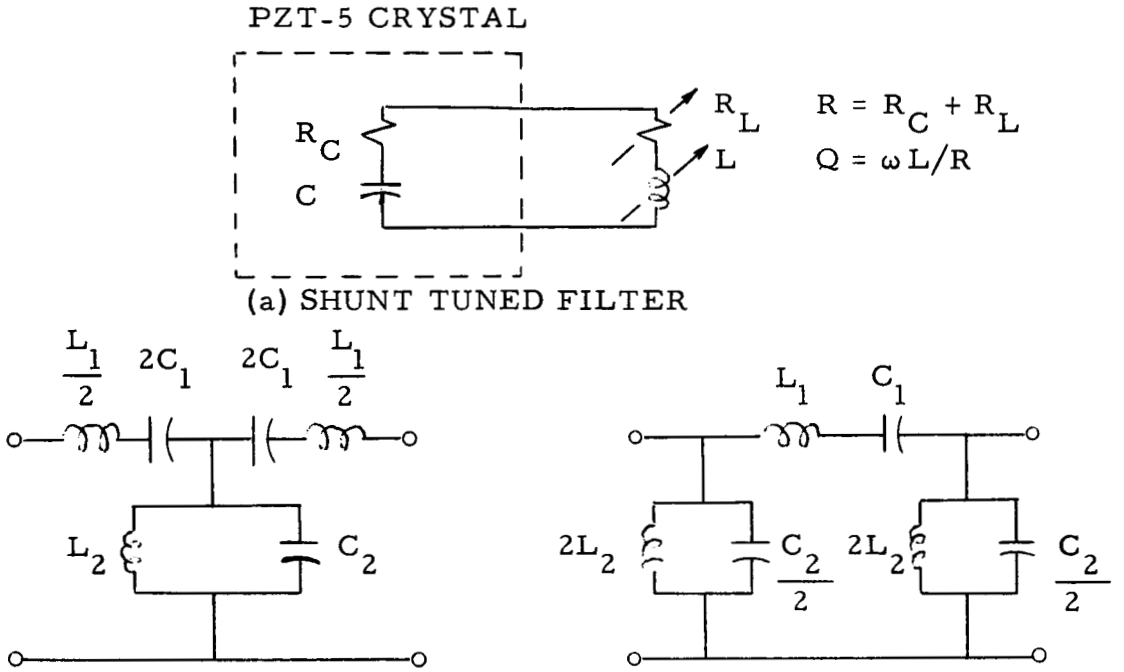

Figure 17. THREE TYPES OF ELECTRICAL FILTERS

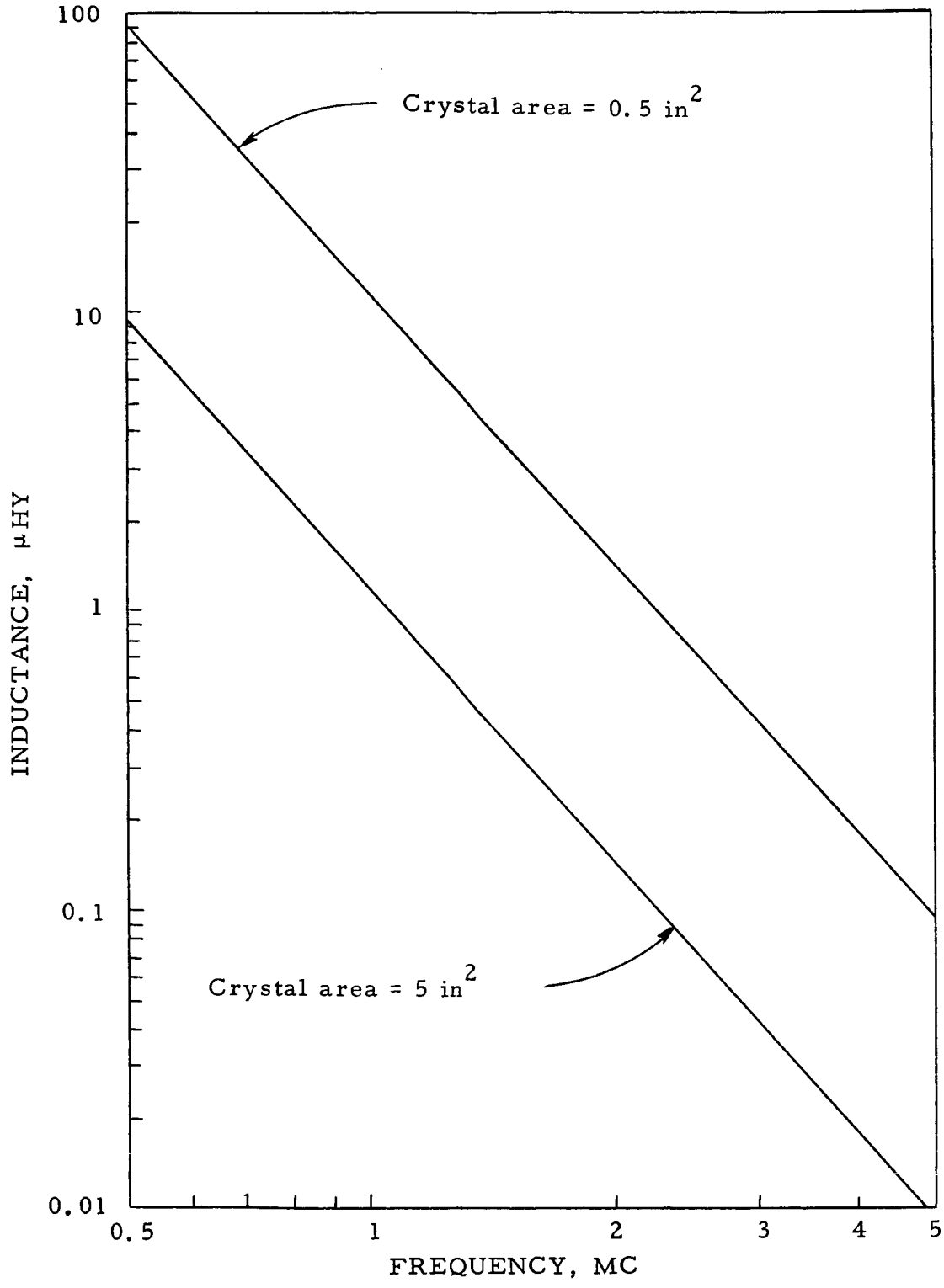

Figure 18. INDUCTANCE REQUIRED TO RESONATE WITH PZT-5 PIEZOELECTRIC CRYSTALS

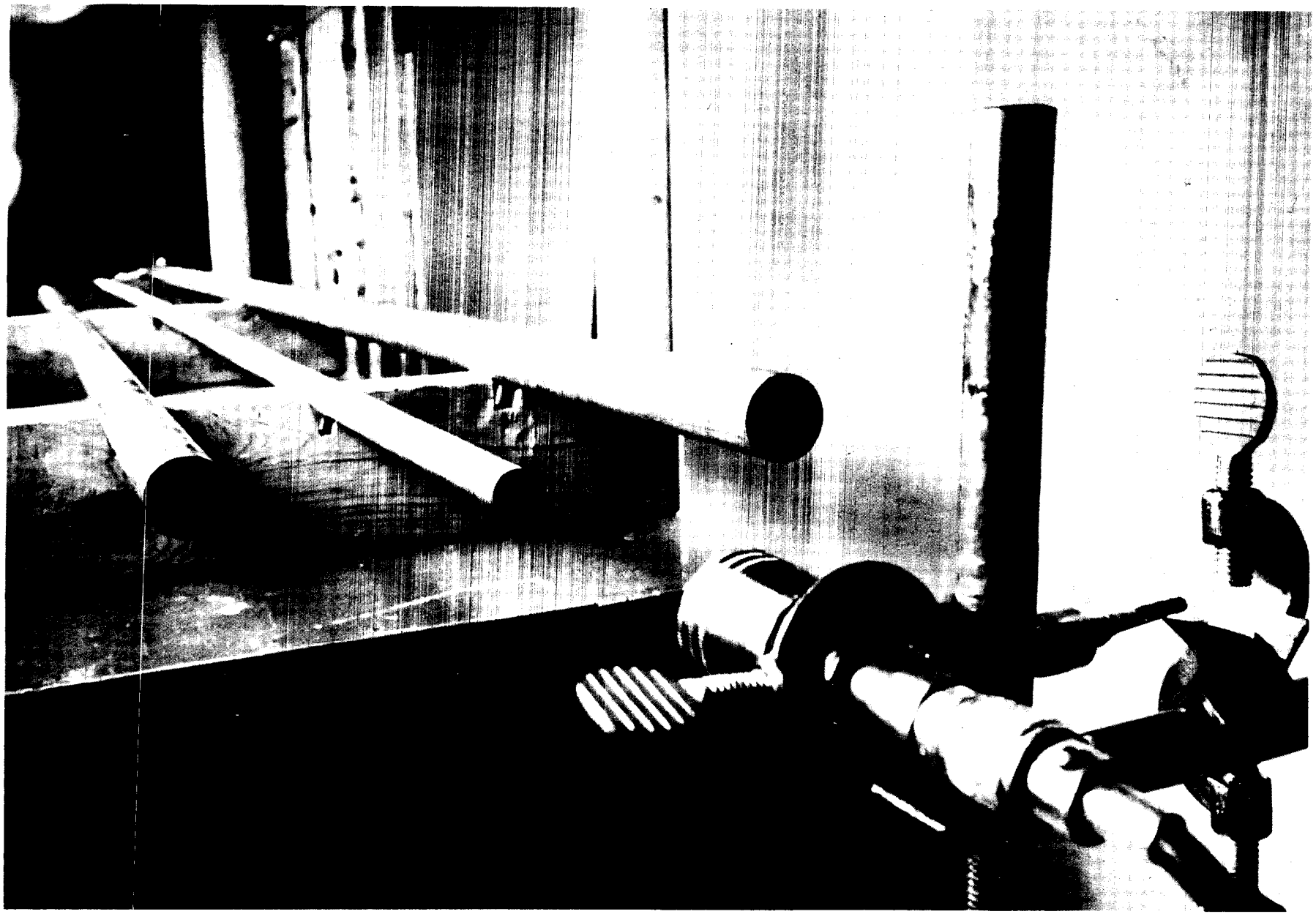

Figure 19. ULTRASONIC TRANSMISSION THROUGH WAVEGUIDES AND AIR

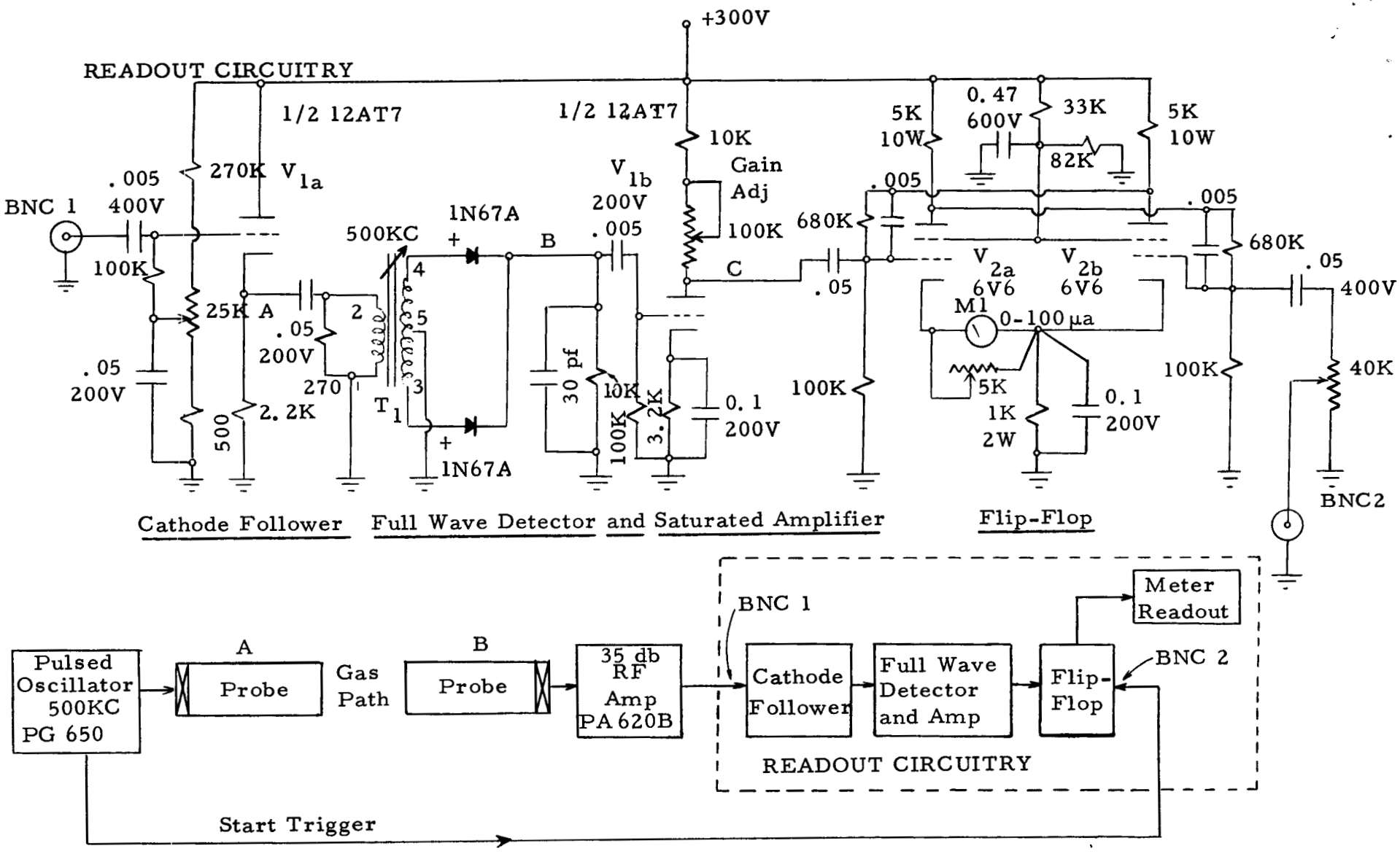

Note: All capacitances in μf unless otherwise noted.
All resistors in ohms unless otherwise noted.

Figure 20. ULTRASONIC THERMOMETER BLOCK DIAGRAM AND READOUT CIRCUITRY

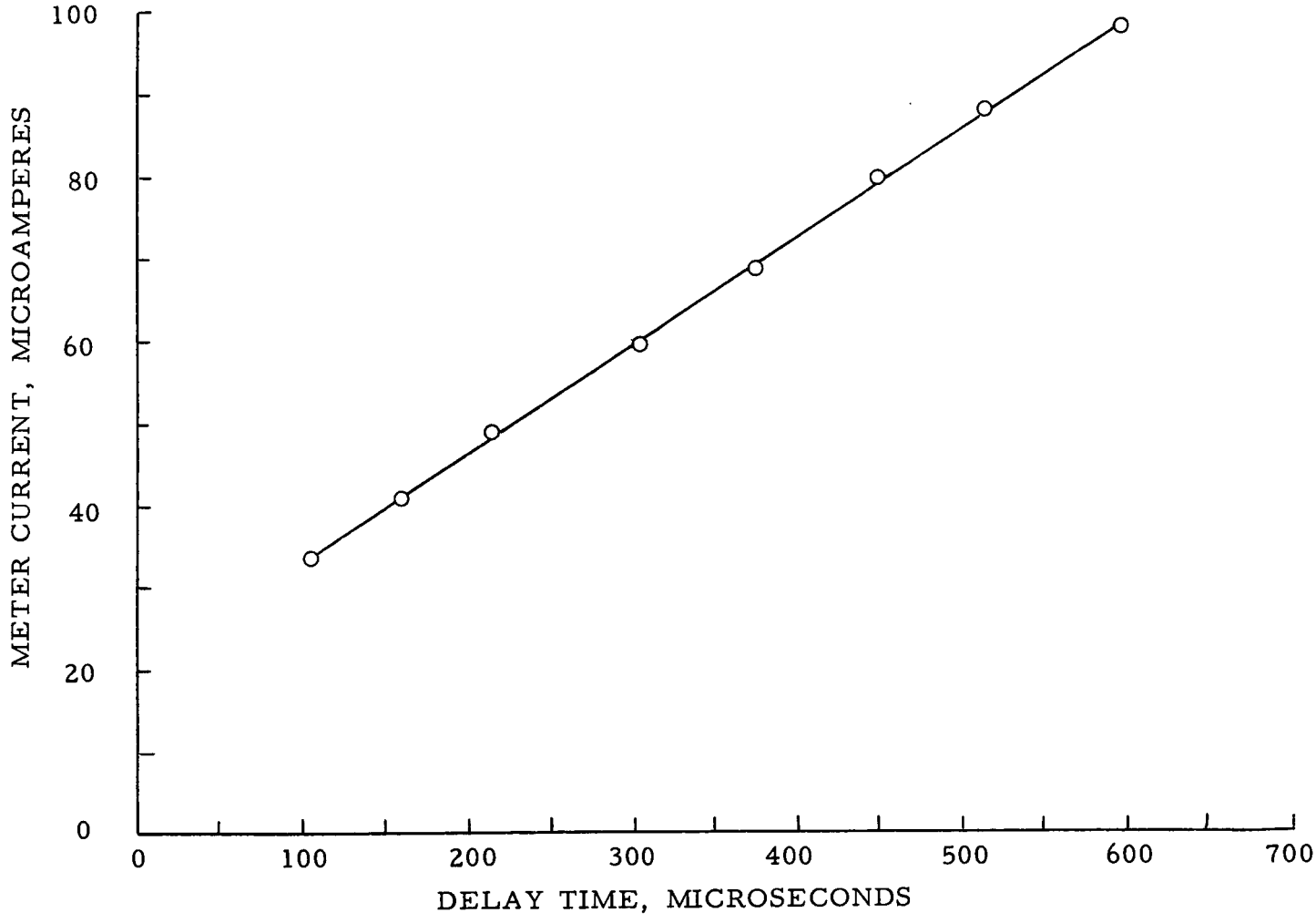

Figure 21. PRELIMINARY CALIBRATION

X. REPORT DISTRIBUTION LIST FOR CONTRACT NO. NAS 3-5201

NASA-Lewis Research Center
21000 Brookpart Road
Cleveland, Ohio 44135
Attention: Miles O. Dustin (10)

NASA-Lewis Research Center
21000 Brookpark Road
Cleveland, Ohio 44135
Attention: Norman T. Musial (1)

NASA-Lewis Research Center
21000 Brookpark Road
Cleveland, Ohio 44135
Attention: Adolph Lovoff
SNPO (2)

National Aeronautics and
Space Administration
Washington, D. C. 20546
Attention: James E. Danberg,
RRP (2)

NASA Ames Research Center
Moffett Field, Calif. 94035
Attention: Library (1)

NASA Goddard Space Flight Center
Greenbelt, Md. 20771
Attention: Library (1)

NASA Langley Research Center
Langley Station
Hampton, Va. 23365
Attention: Library (1)

NASA Marshall Space Flight Center
Huntsville, Ala. 35812
Attention: Library (1)

NASA-Lewis Research Center
21000 Brookpark Road
Cleveland, Ohio 44135
Attention: John J. Fackler
AD&E Procurement Sec. (1)

NASA-Lewis Research Center
21000 Brookpark Road
Cleveland, Ohio 44135
Attention: Library (5)

National Aeronautics and
Space Administration
Washington 25, D. C. 20546
Attention: NPO/F.C. Schwenk (3)

NASA-Lewis Research Center
21000 Brookpark Road
Cleveland, Ohio 44135
Attention: Office of Reliability
and Quality Assurance (3)

NASA Flight Research Center
P. O. Box 273
Edwards, Calif. 93523
Attention: Library (1)

NASA Manned Spacecraft Center
Houston, Texas 77001
Attention: Library (1)

NASA Western Operations
150 Pico Blvd.
Santa Monica, Calif. 90406
Attention: Library (1)

Jet Propulsion Laboratory
4800 Oak Grove Dr.
Pasadena, Calif. 91103
Attention: Library (1)

Battelle Memorial Institute
505 King Avenue
Columbus, Ohio
Attention: John Van Orsdel (1)

Westinghouse Astronuclear Laboratory
Large, Pennsylvania
Attention: R. L. Ramp (1)

Advanced Technology Laboratories
369 Whisman Road
Mountain View, Calif.
Attention: John Chambers (1)

Minneapolis Honeywell
2600 Ridgway Road
Minneapolis 40, Minn.
Attention: F. W. Kuether (1)

Bell Aerosystems Co.
P. O. Box 1
Buffalo 5, New York
Attention: J. V. Robinson (1)

Bendix Research Division
Southfield, Michigan
Attention: D. J. Niehaus (1)

NASA Scientific and Technical Information Facility
Box 5700
Bethesda, Maryland
Attention: NASA Representative(6)

U. S. Atomic Energy Commission
Technical Reports Library
Washington, D. C. (3)

U. S. Atomic Energy Commission
Technical Information Service Extension
P. O. Box 62
Oak Ridge, Tennessee (3)

Battelle Memorial Institute
505 King Avenue
Columbus, Ohio
Attention: REIC (1)

Aerojet General Corporation
Sacramento, Calif.
Attention: T. F. McGrath (1)

Rocketdyne
6633 Canoga Avenue
Canoga Park, Calif.
Attention: John Perow (1)

General Electric Co.
Advanced Technology Service
Cincinnati 15, Ohio
Attention: W. E. Niemuth (1)

Rosemount Engineering Co.
4900 West 78th Street
Minneapolis 24, Minn. (1)

General Electric Co.
5100 West 164th Street
Cleveland, Ohio 44135
Attention: M. Toth (1)

NASA-Lewis Research Center
21000 Brookpark Road
Cleveland, Ohio 44135
Attention: Report Control Office (1)
Nuclear Rocket Technology Office (1)
Dr. John C. Liwosz (1)

Wright-Patterson Air Force Base
Air Force Flight Dynamics Laboratory
Dayton, Ohio
Attention: H. Snowball (1)

Aerojet-General Corporation
Building 2019A2
Department 7411
Sacramento, California
Attention: Dr. K. Sato (1)

Los Alamos Scientific Laboratory
Group N4/P. O. Box 1663
Los Alamos, New Mexico 87544
Attention: Dr. Joseph Perry, Jr. (1)

NASA Headquarters
Washington, D. C. 20546
Attention: John E. Morrissey (1)